Climate Dynamics
https://doi.org/10.1007/s00382-023-06955-9

Summer upper-level jets modulate the response of South American climate to ENSO

Soledad Collazo[1,2] · **Ricardo García-Herrera**[1,3] · **David Barriopedro**[3]

Received: 8 June 2023 / Accepted: 6 September 2023

Abstract
The upper-level jet stream is a critical element of atmospheric circulation, driving synoptic systems and extreme weather events. This study analyzes the impact of upper-level jets on South American (SA) summer temperature and precipitation under different El Niño-Southern Oscillation (ENSO) phases. Using the ERA5 reanalysis dataset from 1979 to 2022, we perform a daily multiparametric characterization of the jet stream, considering its spatial and temporal discontinuities. Besides latitude and intensity, we find that the departure and number of branches of the subtropical jet (STJ) and the longitudinal extent of the Pacific branch of the polar front jet (PFJ) are needed for their description. An additional parameter is required to characterize the STJ due to its absence on around 40% of summer days over SA. Moreover, we observe distinct long-term changes in PFJ parameters across different ocean basins. Three synoptic weather types (WTs) of the upper-level zonal wind are identified: normal conditions, a prominent STJ pattern, and a PFJ-only pattern. The latter pattern is associated with anticyclonic anomalies at 500 hPa in the South Atlantic Ocean and an active SA Convergence Zone, which favors clear skies and warm (wet and cold) conditions in southern SA (Brazil). Consistently, the probability of experiencing warm spells in central Argentina is increased more than twofold. Finally, we detect that the temperature anomalies associated with the WTs are independent of the ENSO phase. However, ENSO modulates the frequency of the WTs: during La Niña (El Niño), the PFJ-only (prominent STJ) pattern is more common.

Keywords Subtropical and polar front jet · Multiparametric characterization · Weather regimes · Extreme temperatures · El Niño-Southern Oscillation · South American summer climate

1 Introduction

Upper-level jet streams are an essential feature of atmospheric circulation at the synoptic scale, playing a key role in the formation and development of mid-latitude cyclones (Holton and Hakim 2013). They are associated with extreme weather phenomena such as heat waves, droughts, and heavy precipitation (Koch et al. 2006; Harnik et al. 2016; Mann et al. 2017; Rusticucci et al. 2017; Collazo et al. 2019a, b; Barriopedro et al. 2022, 2023; Martinez and Solman 2022). Jet streams can be defined as fast and relatively narrow air currents that extend for thousands of kilometers, typically located near the tropopause level (Pena-Ortiz et al. 2013). Upper-level jet streams can be broadly categorized into two main types based on their position and development mechanism: the subtropical jet (STJ) and the eddy-driven jet or polar front jet (PFJ). The STJ typically develops on the poleward side of the Hadley cell due to angular momentum transport (Held and Hou 1980; Hoskins et al. 1983), and the PFJ is commonly located at mid-latitudes, where the presence of a sharp temperature gradient creates favorable conditions for its formation (Pena-Ortiz et al. 2013). In the Southern Hemisphere (SH), the climatology of jet streams exhibits seasonal variations. In the warm season, a single jet dominates the zonal mean across the entire hemisphere,

✉ Soledad Collazo
scollazo@ucm.es

[1] Departamento de Física de la Tierra y Astrofísica, Facultad de Ciencias Físicas, Universidad Complutense de Madrid (UCM), Plaza Ciencias 1, 28040 Madrid, Spain

[2] Departamento de Ciencias del Atmósfera y los Océanos, Facultad de Ciencias Exactas y Naturales, Universidad de Buenos Aires, Buenos Aires, Argentina

[3] Instituto de Geociencias (IGEO), Consejo Superior de Investigaciones Científicas - Universidad Complutense de Madrid (CSIC-UCM), C / Doctor Severo Ochoa 7, Madrid, Spain

Published online: 26 September 2023

whereas autumn and winter exhibit a distinct double jet structure (Gallego et al. 2005).

The upper-level jet streams can also exhibit zonal asymmetries caused by stationary waves that result from topography and heating (Hoskins and Valdes 1990; Held et al. 2002; Lee and Kim 2003). These asymmetries can result in a fragmented or branched structure of the jet streams that can merge again after thousands of kilometers (Pena-Ortiz et al. 2013). In South America (SA), the Andean Mountains, which extend primarily in a north–south direction along the western coast of the continent, significantly perturb the atmospheric circulation favoring the disruption of the upper-level jets (Garreaud 2009). The climatology of the upper-level zonal wind during the summer in SA shows that the mid-latitude zonal flow decelerates over the southern South American continent, after passing through the Andes, and then accelerates over the Atlantic Ocean, where it reaches its maximum intensity (Fig. 1). In addition, a local maximum of the zonal wind is also present north of 40ºS east of the Andes, particularly over central Argentina, which is comparatively weaker in intensity than the mid-latitude jet stream.

Jet-stream research most often involves an analysis of characteristics in terms of the latitudinal position of the jet and the wind speed on its axis (Blackmon et al. 1977; Kidson 1999; Bracegirdle et al. 2018, 2020; Zolotov et al. 2018). However, recent studies have shown that characterizing the complex spatial variability of jet streams using only latitude and intensity is insufficient. To address this issue, researchers have proposed metrics that describe relevant aspects of the PFJ in the Northern Hemisphere (NH), such as tilt (Woollings and Blackburn 2012; Messori and Caballero 2015) or the waviness of the associated mid-latitude circulation (Cattiaux et al. 2016; Di Capua and Coumou 2016; Chen et al. 2016). Barriopedro et al. (2022) demonstrated that a multiparametric approach, incorporating factors such as intensity, sharpness, location, edges, tilt, and zonal asymmetries, can help identify PFJ structures in the NH. On the other hand, Manney and Hegglin (2018) emphasize the importance of making a 3D characterization of jet cores in terms of location (altitude and latitude) and intensity as a function of longitude in both hemispheres. They state that a regional and seasonal breakdown of the jet configuration is necessary to detect changes that may be diluted or masked in areal and seasonal averages. This regional approach to analyzing zonal flow has the advantage of taking into account the influence of topography and land mass distribution (Hoskins and Valdes 1990; Held et al. 2002).

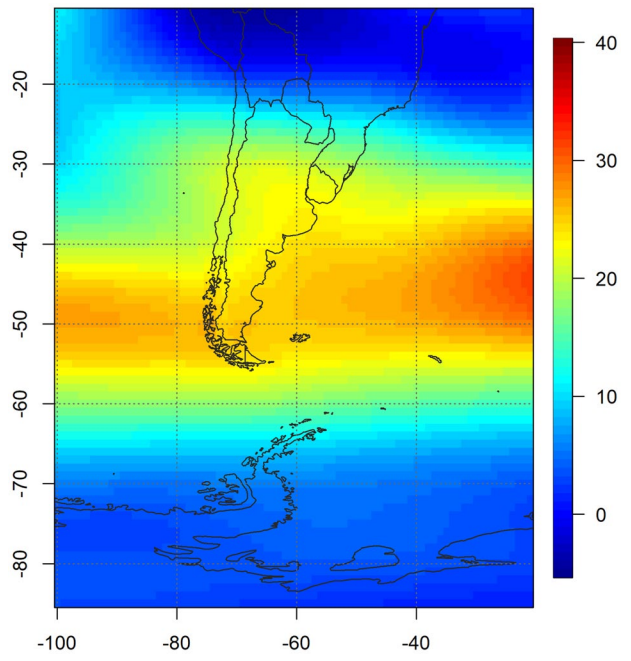

Fig. 1 Climatology of the weighted vertically averaged zonal wind [m/s] between 400 and 100 hPa during the austral summer in the period 1979–2022

Upper-level jets also exhibit temporal variability at multiple scales. Long-term changes since 1979 due to climate change and ozone depletion have been associated with a poleward shift of the PFJ in the SH (Pena-Ortiz et al. 2013; Manney and Hegglin 2018; WMO 2018). However, Banerjee et al. (2020) found that this trend ceased in the December-January–February (DJF) period after 2000. The poleward movement of midlatitude jet streams is consistent with the expansion of the tropical circulation (Lucas et al. 2014). Moreover, modeling studies indicate that the poleward shift of the SH edge of the tropics has been increased by chemical ozone depletion, especially during austral summer, and will be somewhat reversed by the recovery of the ozone hole (Son et al. 2010; Arblaster et al. 2011; McLandress et al. 2011). Regarding the STJ, wind speed has generally increased in winter and decreased in summer (Manney and Hegglin 2018). Observations of upper-level winds indicate positive trends in the upper troposphere (200 hPa) in northern Argentina, and significant positive wind speed trends at most levels in Patagonia's wind profile (Merino and Gassmann 2022). Altitude shifts in both jets during DJF are consistently positive in the SH among different reanalyses, except near the date line (Manney and Hegglin 2018). A recent study concluded that anthropogenic greenhouse gas emissions are the likely driver of the lifting and shifting polewards of the jet streams, although natural variability and the effects of ozone loss may have played some role in this change (Woollings et al. 2023).

On an interannual scale, multiple studies have shown that El Niño-Southern Oscillation (ENSO) can influence the activity of synoptic disturbances. The ENSO is the dominant mode of low-frequency climate variability, typically persisting for several months to a few years. Through Rossby wave propagation, it affects the atmospheric circulation around

the world (Trenberth et al. 1998; Sarachik and Cane 2010). ENSO also has a strong impact on the intensity and location of the STJ, as demonstrated by Yang and Webster (1990). During an El Niño event, the tropical troposphere experiences warming, which strengthens and contracts the Hadley Circulation, resulting in the STJ shifting equatorward (Choudhury et al. 2021). Additionally, there is a significant correlation between ENSO and the upper-level zonal wind, resulting in a stronger Pacific PFJ during La Niña periods and a weaker PFJ during El Niño (Ding et al. 2012).

The ENSO is known to have a significant impact on temperature and precipitation patterns in SA. During El Niño, the Amazon and northeastern SA typically experience drought, while flooding occurs in the tropical west coast and southeastern SA (Montecinos et al. 2000; Barreiro 2010; Cai et al. 2020). Cooler surface-air temperatures in southeastern SA coincide with increased rainfall due to cloud radiative impacts on insolation, although more rainfall often accompanies the enhanced northerly flow of warm air, resulting in low-amplitude air-temperature anomalies. Rusticucci et al. (2017) found that the impact of El Niño events on extreme temperatures in Argentina varies monthly, with colder conditions in the austral summer (fewer warm and more cold days). La Niña, on the other hand, leads to increased frequency of warm days in December, January, and February, and fewer cold days in December and February. Moreover, the frequency of extreme precipitation events in several regions of SA is significantly influenced by the ENSO phases (Grimm and Tedeschi 2009).

Several studies also indicate that the upper-level jet streams influence the temperature and precipitation in SA during the austral summer. Barros et al. (2002) found a strong association between the intensification (reduction) and the northward (southward) shift of the maximum westerly wind over the subtropical latitudes of SA and cold (warm) anomalies of surface temperature in practically every month of the year, at monthly and seasonal scales. Rusticucci et al. (2017) observed significant positive (negative) correlations between the intensity of the jet and cold (warm) extreme indices over several months. A lagged analysis showed that an above-normal intensity of the STJ in November is associated with a lower (higher) occurrence of warm days in northeastern (northwestern) Argentina during summer (Collazo et al. 2019a). Zamboni et al. (2010) demonstrated the existence of a significant simultaneous correlation between bimonthly mean precipitation anomalies over southeastern SA and either the first or the second (depending on the season) leading mode of interannual variability of upper-level wind over SA. More recently, it is identified that the presence of a more intense jet stream at the upper levels of the atmosphere arises as the common feature of extreme rainfall events in southeastern SA (Martinez and Solman 2022).

Temperature and precipitation are influenced by a variety of processes operating at different spatial and temporal scales. Although several studies have shown that the jet streams and ENSO can independently influence these variables, the interplay between these phenomena, particularly in the context of SA, remains a relatively underexplored area of research. Among other factors, Bruick et al. (2019) found that synoptic and thermodynamic conditions favoring deeper storms in SA during El Niño events are associated with a stronger upper-level jet stream, often with the equatorward entry region of the jet stream directly over convective storm regions.

This study aims to analyze the modulation exerted by upper-level jets on the South American summer temperature and precipitation under different ENSO phases, utilizing the ERA5 reanalysis dataset from 1979 to 2022. The study employs a multiparametric daily characterization of the jets, including several parameters that have not been previously used in the region. The statistical characteristics of these parameters, such as their frequency distributions and trends, are explored. A subset of parameters is discerned to establish a refined characterization of the jets, leading to the identification of synoptic weather types (WTs) associated with the zonal wind in the upper troposphere. Furthermore, the influence of WTs on atmospheric circulation is examined through composites of several meteorological variables. Finally, the impact of jet stream patterns on warm spell occurrence is also evaluated.

2 Data and methods

2.1 2.1 Data

To characterize the upper-level jet over SA during the austral summer (DJF), we utilize hourly zonal wind data from the ERA5 reanalysis datasets (Hersbach et al. 2020), for the period 1979–2022 at seven pressure levels ranging from 100 to 400 hPa. The data are obtained from the Copernicus Climate Change Service website (https://cds.climate.copernicus.eu/cdsapp#!/dataset/reanalysis-era5-pressure-levels?tab=overview, accessed in January 2023), and are aggregated into daily values for each pressure level. To facilitate large-scale circulation analysis, the original 0.25ºx0.25º resolution is re-gridded to 1ºx1º using bilinear interpolation. Furthermore, we estimate the mass-weighted vertical mean zonal wind for many of our analyses. As our primary interest is to study the impact of the jet on the climate of SA, we confine our analysis to a region centered on this continent (100º-20ºW, 85-10ºS). We use Climate Data Operator command lines to perform these data processing steps.

Daily data of geopotential height at 500 hPa, minimum and maximum temperature, precipitation, and outgoing

longwave radiation (OLR) from ERA5 are also used to analyze the relationship of the jet with the SA climate. Daily anomalies are estimated as deviations of the climatological period 1991–2020 from the corresponding calendar day. In addition, the CPC daily gridded observational datasets (Xie et al. 2007) are used to contrast the results obtained with the reanalysis for maximum and minimum temperature and precipitation (https://psl.noaa.gov/data/gridded/data.cpc.globaltemp.html, https://psl.noaa.gov/data/gridded/data.cpc.globalprecip.html, accessed in January 2023). CPC data have a longitude-latitude resolution of 0.5ºx0.5º, so the ERA5 data are interpolated to this resolution.

To determine the ENSO phase, we utilize the National Oceanic and Atmospheric Administration (NOAA) Oceanic Niño Index (ONI) for the DJF season (https://origin.cpc.ncep.noaa.gov/products/analysis_monitoring/ensostuff/ONI_v5.php, accessed in February 2023). The ONI is calculated based on the sea surface temperature anomalies in the Niño 3.4 region, which is in the equatorial Pacific Ocean between 120°W and 170°W longitude and 5°N and 5°S latitude. An ONI value greater than or equal to + 0.5 °C indicates El Niño conditions, while a value less than or equal to -0.5 °C indicates La Niña conditions.

2.2 2.2 Multiparametric characterization of the upper-level jets

In this study, we employ a novel daily multiparametric approach to effectively characterize upper-level jets. We adapt the parameters introduced by Barriopedro et al. (2022) for analyzing the NH PFJ to investigate the jet streams in the unique context of SA. Moreover, we incorporate valuable insights from prior studies conducted by Gallego et al. (2005) and Pena-Ortiz et al. (2013), which provide comprehensive descriptions of jets in the SH.

The parameters defined in this work to characterize the upper levels circulation over SA are shown in Table 1. All of them were defined from the vertically averaged zonal wind, except for the parameters indicating the jet altitude. It is often observed that upper-level jets exhibit zonal asymmetries (i.e. there are longitudes where the zonal wind is weakened) within the study region. This generates the presence of several branches in both jets. The presence of the Andes Mountain range plays a relevant role in this jet behavior by causing stationary waves (Hoskins and Valdes 1990; Held et al. 2002; Lee and Kim 2003). Therefore, for each jet branch, the position of the zonal wind maximum on that branch and its intensity are identified. The branches are classified as Atlantic (*atl*) or Pacific (*pac*) according to whether the jet maximum is located east or west of 70ºW (longitude where the Andes Mountains are located approximately) respectively.

As an example, Fig. 2a illustrates the zonal wind field for 19 January 1986 and the identification of some of the jet parameters. The STJ presents a single branch with a jet maximum located in the Atlantic Ocean very close to the SA coast. This branch has a slightly negative tilt and a longitudinal extent of 56º. The PFJ has two branches, one located in the Pacific Ocean and the other one in the Atlantic Ocean. The former has a positive tilt, while the latter has a negative tilt. It can also be seen that the Pacific branch has a greater longitudinal extension and is slightly more intense than the Atlantic branch in this particular day. The zonal mean of the zonal wind shows that the 30 m/s threshold is exceeded at two different latitudes, one north of 40ºS and the other south, close to 55ºS (Fig. 2b). It is also observed that the PFJ has a greater latitudinal extent than the STJ, and that lat.pfj (blue solid line) is closer to the southern flank (lats.pfj) than to the northern one (latn.pfj).

2.3 2.3 Analysis of the upper-level jet parameters

First, we describe the austral summer daily distributions of the jet parameters through probability density functions and boxplots. The Kolmogorov–Smirnov test (KS test) is used to test whether the data distributions come from the same population (Smirnov 1948). A bootstrap version of the univariate KS test is performed to establish the statistical significance using 5000 Monte Carlo simulations.

We also study long-term changes in the jet parameters over the period 1979–2022. The non-parametric Mann–Kendall trend test (Mann 1945; Kendall 1975), and Sen's slope estimator are employed to estimate the magnitude of the trend (Sen 1968). Later, we filter these trends by subtracting the linear regression from the original parameters. From the detrended parameters, Spearman's correlation coefficient between all parameters is estimated (Spearman 1904). It is expected that many of these parameters are associated (e.g., *lat* and *latn*), so we can retain only a subset of parameters according to their correlation matrix. To accomplish this, we apply the Partitioning Around Medoids (PAM) algorithm (Kaufman and Rousseeuw 1990). PAM is a non-hierarchical algorithm that works by iteratively optimizing the selection of medoids, which are representative objects that minimize the average dissimilarity between themselves and the other objects within a given cluster. The number of medoids must be defined by the user prior to applying the algorithm. PAM is more robust than other clustering algorithms to noise and outliers in the data, and it can handle a variety of dissimilarity measures. In our study, the input data for the PAM algorithm is the dissimilarity matrix obtained from the correlation matrix of the detrended upper-level jet parameters following the Eq. (1). The Calinski-Harabasz metric, also known as pseudo-F statistic (Calinski and Harabasz 1974), is used to determine the optimal number of clusters (Eq. 2).

Table 1 Definition of the jet parameters used in this work

	Parameter	Acronym	Definition	Units
From the zonal mean of the zonal wind [U]	Latitudinal position	Lat	lat is the latitude where a local maximum of [U] is found. The local maximum must satisfy that: 1. [U] > 30 m/s 2. The distance between two local maxima is at least 15º 3. Two local maxima are allowed in order to represent the STJ and PFJ If there is only one local maximum, it is classified as STJ or PFJ considering 40ºS as the latitude limit (Gallego et al. 2005; Pena-Ortiz et al. 2013). Pena-Ortiz et al. (2013) found a minimum of the zonal integral of the probability of occurrence of jet cores at this latitude in the SH and observed that this value is independent of the season	º
	Wind speed	Int	*int* is simply [U] at *lat*	*m/s*
	Sharpness	Shar	*shar* is defined as the difference between *int* and the meridional mean of [U]	*m/s*
	Poleward latitude	Lats	Southern flank of the jet defined as the latitude south of *lat* where the [U] values have decreased by half the *shar*	º
	Equatorward latitude	Latn	Northern flank of the jet defined as the latitude north of *lat* where the [U] values have decreased by half the *shar*	º
Without the estimation of zonal means	Tilting	Tilt	*tilt* is defined as the slope of the linear regression between latitudes meeting the same criteria as *lat* and longitudes. Additionally, it is required that between two consecutive longitudes, the latitude does not vary by more than 2° (or twice the resolution of the data) and that the longitude extension of the jet branch is greater than 10° to avoid calculating a regression with too little data	º / º
	Departure	Dep	*dep* is then computed as the root mean squared difference of the latitude at which the maximum of the jet is located at each longitude and *lat*. The departure parameter measures the degree of complexity of the jet in the latitudinal direction	º
	Branches	branches	number of STJ and PFJ divisions	
	Longitude position in the Pacific	lon.pac	Longitudinal position of the zonal wind maximum in the Pacific branch	º
	Longitude position in the Atlantic	lon.atl	Longitudinal position of the zonal wind maximum in the Atlantic branch	º
	Latitude position in the Pacific	lat.pac	Latitudinal position of the zonal wind maximum in the Pacific branch	º
	Latitude position in the Atlantic	lat.atl	Latitudinal position of the zonal wind maximum in the Atlantic branch	º
	Wind speed in the Pacific	int.pac	Intensity of the zonal wind maximum in the Pacific branch	m/s
	Wind speed in the Atlantic	int.atl	Intensity of the zonal wind maximum in the Atlantic branch	m/s
	Longitude extension in the Pacific	ext.lon.pac	Extension in the longitudinal direction of the Pacific branch and over which the *tilt* is estimated	º
	Longitude extension in the Atlantic	ext.lon.atl	Extension in the longitudinal direction of the Atlantic branch and over which the *tilt* is estimated	º
	Height in the Pacific	hei.pac	Pressure level at which the maximum zonal wind is located at (*lon.pac, lat.pac*)	hPa
	Height in the Atlantic	hei.atl	Pressure level at which the maximum zonal wind is located at (*lon.atl, lat.atl*)	hPa

Milligan and Cooper (1985) establish that the pseudo-F statistic is one of the more effective procedures for determining the number of clusters according to a comprehensive evaluation of more than 30 methods. This metric has already been used to determine the number of clusters of meteorological data (Bettolli et al. 2010; Penalba et al. 2013).

$$Dissimilarity = 1 - abs(correlation) \quad (1)$$

$$PseudoF = \frac{B(n-k)}{W(k-1)} \quad (2)$$

where B is the between-cluster sum of squares, W is the within-cluster sum of squares, k is the number of clusters, and n is the total number of observations.

We also employ the PAM algorithm to identify the recurrent synoptic WTs of the zonal wind at upper levels. This algorithm is applied to the daily parameters that are identified as medoids, allowing us to group together days that

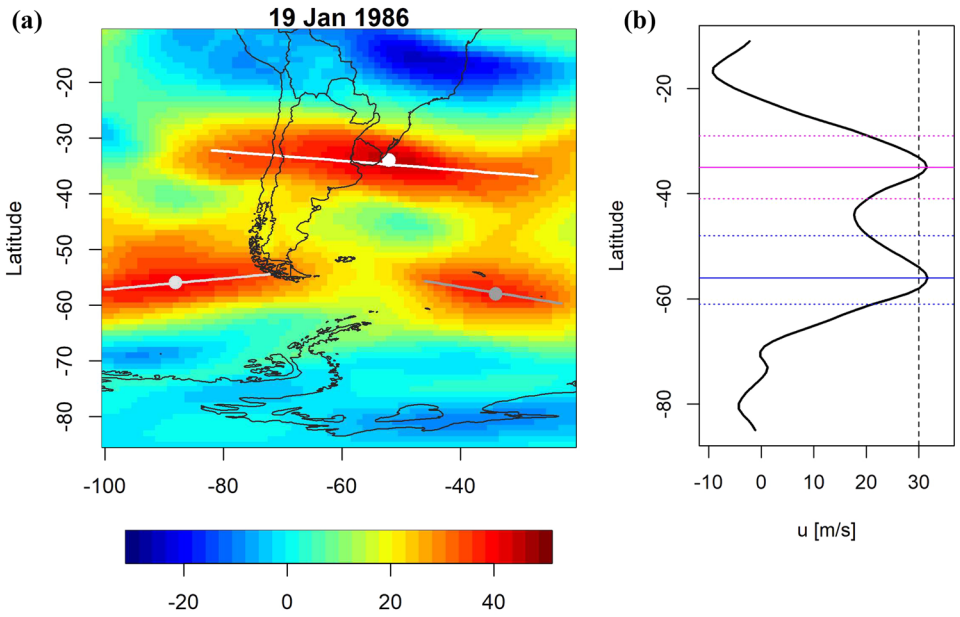

Fig. 2 Example of the diagnosis of jet parameters for 19 January 1986. Vertically averaged zonal wind between 400 and 100 hPa (**a**). The points indicate the location of the maximum zonal wind and lines linear regression representing the tilting the at each branch (white: subtropical jet, gray: polar front jet). Zonal mean of the zonal wind (**b**). Dashed vertical line is the threshold to determinate the jet presence. The horizontal solid line identifies the latitude (lat) and dashed lines correspond to the northern and southern flanks (latn and lats) of the subtropical jet (magenta) and polar front jet (blue)

exhibited similar conditions in terms of these central parameters. The use of only these central parameters to cluster summer days with similar jet configurations allows us to reduce the complexity of the problem and the number of dimensions involved. By utilizing this approach, we aimed to uncover distinct clusters of synoptic patterns that can provide valuable insights into the underlying dynamics and variability of the zonal wind. The assignment of each day to a cluster is accomplished using a dissimilarity metric. The selection of a distance measure should be based on the specific objectives of the study and the types of variables involved since different measures capture different aspects of similarity or dissimilarity between variables. In this case, we utilized the versatile Gower distance (Gower 1971) to obtain the dissimilarity matrix, as it can handle various types of variables, missing data, and scale variables based on their range to give them equal weight in the distance calculation. Therefore, the Gower distance relies on different types of information from n variables to measure the similarities between two individuals.

2.4 2.4 Influence of Upper-Level Jets and ENSO on South American weather

Days grouped based on upper-level jet synoptic patterns are used to create composites of anomalies in several variables, including geopotential height at 500 hPa, minimum and maximum temperature, precipitation, and OLR. The anomalies are assessed for statistical significance using a Student's test at a 95% confidence level. Additionally, composite analyses of these variables are performed, considering not only the zonal wind pattern but also the phase of the ENSO. Significance tests with a Student's test are also applied to evaluate if these composites significantly differ from the ENSO climatology in the region.

Finally, the relationship between the WTs of the zonal wind and the occurrence of warm spells (WS) is analyzed. A WS is defined when the maximum temperature exceeds the daily 90th percentile of its distribution (warm day) for at least three consecutive days. To estimate this percentile, a 5-day window centered on each calendar day and the base period 1991–2020 is considered. In this period, by definition, the number of warm days is expected to be 10%. However, in our work we used this threshold to detect warm days over a longer period, 1979–2022. Due to the non-stationarity of the climate, the value of 10% of days can be significantly modified.

The probability of occurrence of a day with WS conditioned to a specific WT of the upper-level jet is compared to the climatological probability of its occurrence. The Z-statistic (Eq. 3) is used to quantify the difference in probabilities (Infante Gil and Zárate de Lara 1984).

$$Z = \frac{p_1 - p_2}{\sqrt{\frac{p_1(1-p_1)}{n_1} + \frac{p_2(1-p_2)}{n_2}}} \tag{3}$$

where p_1 is the conditional probability of occurrence of a day with WS conditioned to a given synoptic pattern of the upper-level jet, and p_2 is the climatological probability estimated as the ratio between the total number of days with WS and the total sample size. This analysis is repeated by comparing against the climatological probability of WS in each ENSO phase.

3 Results

3.1 3.1 Analysis of the jet parameters

First, we describe the daily summer distributions of the jet parameters obtained from the zonal mean of the zonal wind. The intensity and sharpness distributions of the PFJ exhibit significant differences compared to the STJ. The PFJ displays higher intensities, occasionally reaching or surpassing 50 m/s (Fig. S1). Regarding the latitudinal parameters, *lat* and *latn*, the STJ shows relatively less variability, with a mean latitude of approximately 35ºS, while its northern edge is situated around 29ºS. In contrast, the central latitude of the PFJ displays greater variability and elevated values of *dep*. On the other hand, the southern edge of the STJ shows a higher variability compared to the PFJ.

The distributions of the parameters characterizing the jet branches in the ocean basins are shown in Fig. 3. The definition of this new set of parameters allows us to reveal and quantify in more detail some of their properties. Many seasonal and hemispheric averaging studies observe the presence of a single summer jet in the SH (Nakamura and Shimpo 2004; Gallego et al. 2005); however, the analysis on a daily scale and focused on the South American region shows that the STJ is present on approximately 60% of the summer days, while the PFJ is consistently present and typically exhibits one or two branches (Fig. 3a,b).

As observed in the zonal averages, both branches of the PFJ tend to be more intense and with greater variability in their latitudinal position than the STJ branches (Fig. 3c–f). Furthermore, we find that the intensity of the Atlantic branch of the STJ (*int.atl.stj*) presents a distribution that differs significantly from the Pacific branch, with *int.atl.stj* reaching higher velocities (Fig. 3c). Note that the Atlantic sector encompasses the continental region east of the Andes, where substantial thermal gradients can arise, thereby intensifying the STJ. This is not observed for the PFJ as the continental area in mid and high latitudes is considerably reduced.

In terms of longitudinal locations, the maximum wind speed of the Pacific branch of the STJ shows a clear preference just west of the Andes (Fig. 3g). This mountain range, with an elevation surpassing 2000 m.a.s.l. in the subtropics, acts as a physical barrier that obstructs the eastward flow and forces it upwards, resulting in a local acceleration of the zonal wind. On the other hand, the Pacific branch of the PFJ shows two preference locations: one in the western boundary of the study region and the other near the Andes (Fig. 3h). Regarding the Atlantic branch of both jets, the longitudinal position of the maximum wind speed presents more variable locations than the Pacific branch. However, it is observed that the STJ has a slightly higher frequency between 60º and 50ºW on the east coast of the continent where thermal contrasts are favored, while the PFJ reaches maximum velocities over the Atlantic Ocean (at the eastern limit of the studied region) which coincides with what is observed in the climatological field (Fig. 1). The longitudinal extent of both branches is usually greater in the PFJ (Fig. 3i, j) because it is less influenced by the presence of the continent.

The jet stream forms meanders that occur between alternating high-pressure ridges and low-pressure troughs (Janach 2015), which favors the tilting of the jets. A negative tilt implies a NW–SE orientation of the jet branches and is compatible with the expected inclination at the front of the trough. As observed by Barriopedro et al. (2022) for the NH PFJ, the tilt displays a near-Gaussian distribution for all the branches, with frequency maxima at slightly negative values, especially for STJ (Fig. 3k,l).

Finally, it is found that the STJ is located at higher altitudes than the PFJ because the thickness of the troposphere increases as we move towards the equator (Fig. 3m, n). As we have seen, the PFJ presents a large latitudinal variability that will also be accompanied by a greater variability in the jet altitude. The behavior of this parameter does not usually show marked differences between the Atlantic and Pacific branches.

To continue with the statistical description of these jet stream parameters, an analysis of the trends of the summer aggregate values of these parameters for the period 1979–2022 is carried out. The results indicate significant changes at the 5% level mainly for the PFJ parameters (Table 2). The PFJ shows a poleward shift and an ascent into the upper levels of the atmosphere in SA, which is robust to results previously obtained for other reanalyses (Pena-Ortiz et al. 2013; Manney and Hegglin 2018; WMO 2018). Climate warming favors an expansion of the tropical circulation (Lucas et al. 2014) and an increase in the altitude of the tropopause (Santer 2003; Lorenz and DeWeaver 2007; Seidel and Randel 2007; Archer and Caldeira 2008; Xian and Homeyer 2019). The introduction of newly defined parameters allows us to make significant additional observations on the changes in the PFJ over the last decades. Distinguishing differences emerge between the Atlantic and Pacific branches. We observe a substantial poleward displacement exclusively within the Pacific branch of the PFJ. Conversely, the Atlantic branch exhibits a prominent acceleration of the jet exceeding 0.5 m/s per decade—approximately twice the observed trend in zonal mean wind speed. Regarding the jet altitude, substantial changes are observed in both branches, but the Atlantic branch stands out with a more pronounced ascent. Moreover, our analysis reveals an amplified variability in the latitudinal position of the PFJ within the studied region. This is attributed to the contrasting behavior

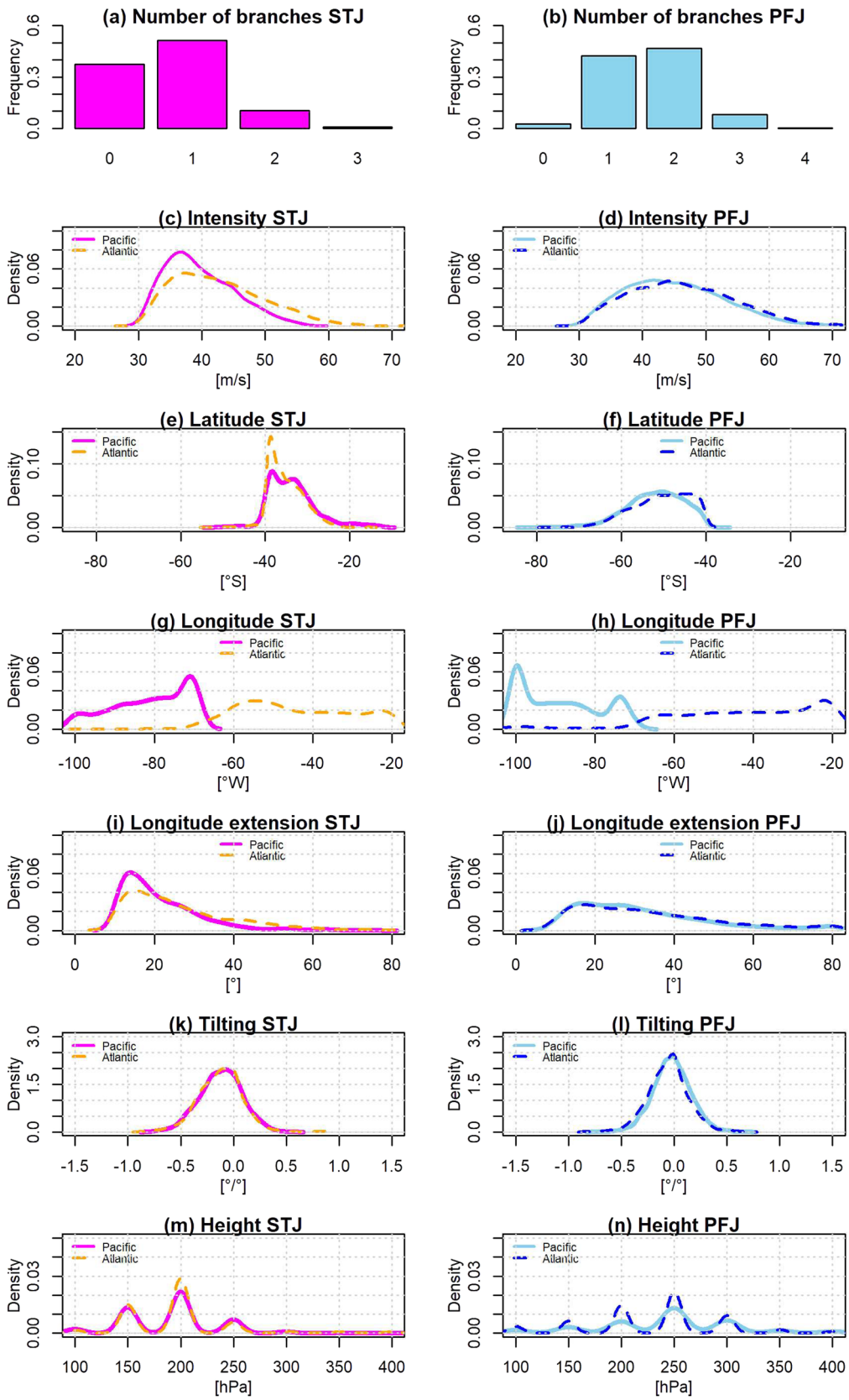
(a) Number of branches STJ
Frequency
0.0
0.3
0.6
0
1
2
3
(b) Number of branches PFJ
Frequency
0.0
0.3
0.6
0
1
2
3
4
(c) Intensity STJ
Density
0.00
0.06
Pacific
Atlantic
20
30
40
50
60
70
[m/s]
(d) Intensity PFJ
Density
0.00
0.06
Pacific
Atlantic
20
30
40
50
60
70
[m/s]
(e) Latitude STJ
Density
0.00
0.10
Pacific
Atlantic
-80
-60
-40
-20
[°S]
(f) Latitude PFJ
Density
0.00
0.10
Pacific
Atlantic
-80
-60
-40
-20
[°S]
(g) Longitude STJ
Density
0.00
0.06
Pacific
Atlantic
-100
-80
-60
-40
-20
[°W]
(h) Longitude PFJ
Density
0.00
0.06
Pacific
Atlantic
-100
-80
-60
-40
-20
[°W]
(i) Longitude extension STJ
Density
0.00
0.06
Pacific
Atlantic
0
20
40
60
80
[°]
(j) Longitude extension PFJ
Density
0.00
0.06
Pacific
Atlantic
0
20
40
60
80
[°]
(k) Tilting STJ
Density
0.0
1.5
3.0
Pacific
Atlantic
-1.5
-1.0
-0.5
0.0
0.5
1.0
1.5
[°/°]
(l) Tilting PFJ
Density
0.0
1.5
3.0
Pacific
Atlantic
-1.5
-1.0
-0.5
0.0
0.5
1.0
1.5
[°/°]
(m) Height STJ
Density
0.00
0.03
Pacific
Atlantic
100
150
200
250
300
350
400
[hPa]
(n) Height PFJ
Density
0.00
0.03
Pacific
Atlantic
100
150
200
250
300
350
400
[hPa]

◂**Fig. 3** Frequency bar plot of the number of branches of the jets (**a**, **b**) and climatological mean frequency distributions of the austral summer jet parameters (**c**-**n**) for the 1979–2022 period. The left (right) column shows the parameters for the subtropical (polar) jet. The solid (dashed) lines are used to represent the jet parameters of the Pacific (Atlantic) branch

observed between the Atlantic and Pacific branches. While the Atlantic branch exhibits no significant change in its latitudinal position, the Pacific branch demonstrates a noteworthy poleward shift, contributing to the overall increased spatial variability. Finally, it is highlighted that the weaker and more discontinuous conditions of the STJ, both spatially and temporally, lead to the STJ having less consistent changes than the PFJ during the austral summer. Among all the STJ parameters, we only find an increase in the longitudinal extension of the Pacific branch. This extension could potentially be associated with localized changes in the Hadley cell response to variations in sea surface temperature (Fatmasari 2021). However, further comprehensive studies are required to better understand and explore this phenomenon.

We have gathered a wide range of parameters to characterize STJ and PFJ; however, many of them are likely to show an association. To ensure an accurate estimation of linear associations and avoid spurious correlations, we proceeded to filter the linear trends of the parameters. Numerous significant associations are evident among the defined parameters (Fig. S2). It is noteworthy that these associations extend beyond solely the latitudinal parameters. For instance, the parameters of intensity and sharpness exhibit a positive association, while the departure and tilting of the STJ display a negative correlation. As observed earlier, negative values of inclination are highly favored in the STJ (Fig. 3k), thus a more pronounced NW–SE tilt corresponds to a greater fluctuation in the latitudinal position of the jet.

Therefore, the parameters are not independent and may provide redundant information. The correlation matrix allows us to visualize certain groups of variables that are associated with each other; however, it is difficult to group them directly from this matrix. To achieve this in an objective way, we apply the PAM algorithm to the distance matrix estimated from the correlation matrix. The optimal number of clusters, determined by the Pseudo-F criterion, is found to be 7, as it exhibits a maximum at this value (Fig. S3a). Table 3 presents the central parameter of each cluster (medoids) along with the corresponding parameters encompassed within each cluster. Clusters 1 and 5 predominantly group characteristics associated with the position of the STJ and PFJ, respectively. Clusters 2 and 6 are dominated by parameters linked to wind speed, while Cluster 3 presents several parameters related to *tilt*. Cluster 4 only consists of *branches.stj* and *hei.atl.stj*, which exhibit a significant positive correlation. Finally, Cluster 7 is characterized by parameters associated with the longitudinal position of the PFJ.

The preceding analysis has led us to identify seven key parameters for characterizing the summer jets in SA. Four parameters are needed to effectively describe the STJ, whereas three parameters are sufficient for the PFJ. While the traditional parameters of latitude and intensity hold significance for both jets, they do not provide a complete picture. To enhance the characterization of the PFJ, we include the longitudinal extent of the Pacific branch, which exhibits considerable variability, as depicted by the frequency distributions (Fig. 3j). To capture the complexities of the STJ, it is crucial to consider the *dep* and the number of branches. The number of branches enables a comprehensive analysis of the temporal and spatial discontinuity observed within the STJ during the austral summer, while the *dep* parameter quantifies the latitudinal complexity. An additional parameter is required to accurately capture and quantify its intermittent nature during the summer days (unlike PFJ, which is consistently present).

3.2 3.2 Weather types derived the jets parameters and its influence on the atmospheric circulation.

Based on this new characterization of the jets using four parameters to describe the STJ and three parameters for the PFJ, we can derive synoptic weather types of the zonal wind at upper levels during the summer over SA. These patterns will enable the grouping of summer days that exhibit similar configurations in the jets, facilitating the identification of common atmospheric conditions. The optimum number of WTs is determined to be three from the Pseudo-F statistic (Fig. S3b). For each of these WTs, we can obtain composites of the zonal wind to visualize their spatial configuration (Fig. 4).

WT1 encompasses just over 50% of the summer days, making it the designated "Normal" pattern for the season. In this weather type, the PFJ is characterized by two branches, with one extending over the Atlantic and the other over the Pacific, with the former displaying higher intensity (Fig. 4a). Additionally, a branch of the STJ is observed over central Argentina and Uruguay. This pattern most closely resembles the zonal wind climatology shown in Fig. 1.

WT2 comprises approximately 11% of the summer days and represents a distinctive weather pattern characterized by the prominent influence of the STJ. In this pattern, the STJ is positioned over central Argentina and gradually tilts southeastward over the Atlantic Ocean, attaining its peak intensity. Accompanying this pronounced *tilt*, the *dep.STJ* exhibits higher values compared to the "Normal" pattern, with significantly different distributions (Fig. 4b). Additionally, the circulation of both jets over the Pacific remains

Table 2 Jet parameters with significant trends at 5% in the period 1979–2022 and the Sen's slope estimator

Parameter	Trend	Parameter	Trend
lat.PFJ	− 0.59º per decade	*int.PFJ*	0.24 m/s per decade
lat.pac.PFJ	− 0.55º per decade	*int.atl.PFJ*	0.51 m/s per decade
dep.PFJ	0.18º per decade	*hei.pac.PFJ*	− 3.96 hPa per decade
ext.lon.pac.STJ	0.69º per deacade	*hei.atl.PFJ*	− 4.50 hPa per decade

relatively weak in WT2. In particular, the *int.PFJ* is lower in WT2 and displays a distribution that significantly differs from that observed in WT1 (Fig. 4c).

Finally, WT3, accounting for approximately 37% of summer days, represents a distinct weather pattern where only the PFJ is present, i.e., the STJ is absent. In this WT, the PFJ exhibits a more continuous zonal structure, positioned around 48ºS. WT3 stands out as the most distinctive among the three WTs. This differentiation stems from the absence of the STJ and significant differences in the frequency distributions of all parameters used to describe the PFJ when compared to the other two patterns. It is characterized by a PFJ that tends to have a narrower latitudinal range, higher intensity, and greater longitudinal extent in comparison to the other weather types (Fig. 4c).

An example of the zonal wind field at upper levels for a given day of each WT is shown in Fig. S4. The selected days corresponds to the day with the lowest L1-norm of the difference between the median of the main standardized parameters for each WT and the specific values of these parameters on each day (this measure is called the Manhattan distance).

We now inquire about the persistence and prevailing transitions of these configurations. For each WT, we conduct an identification process for events, characterized as one or more consecutive days classified within that specific WT. To evaluate persistence, we examine the frequency of occurrence of events that have durations equal to *d* days. Analysis of the persistence of the WTs reveals important differences among them (Fig. 5). WT2 has the lowest persistence with no event lasting more than 5 consecutive days and most frequently lasting only one day. In contrast, WT3 shows that several events can persist for more than 5 days, including two record events lasting 17 days. This discrepancy in persistence can be partially attributed to favorable blocking conditions over the Atlantic associated with WT3, as will be presented later in this section. Finally, WT1 presents events that on average have a persistence between 1 and 6 days.

To quantitatively assess the probability of persistence and transitions between the WTs, we calculate the absolute frequencies of evolving from group *i* to group *j* over consecutive days. Using these values, we estimate the conditional probabilities (Table 4). WT1 and WT3 have a probability of remaining in the same cluster of approximately 65%, which is consistent with the higher persistence observed in Fig. 5, while WT2 has only a 31% probability of persistence. In contrast, the most probable transition between patterns occurs from WT2 to WT1, indicating a decrease in the *dep* of the jet stream over the Atlantic and its movement towards higher latitudes. Consequently, only a residual portion of the STJ persists over central Argentina and Uruguay. On the other hand, the probability of a transition from WT3 to WT2 is exceptionally low, estimated at only 3%. This low likelihood arises from the fact that such a transition would involve a sudden emergence of a prominent STJ from a state where it is initially absent. Moreover, the probability of transitions between WT1 and WT3 is higher compared to transitions between WT1 and WT2. This observation indicates that a weakening of the STJ is more likely than an increase in its inclination in the South Atlantic Ocean during the austral summer.

In addition to obtaining the WTs of the upper-level zonal wind, it is possible to derive composites of other meteorological variables to analyze the associated atmospheric circulation and weather conditions. The composite of the 500 hPa geopotential height anomalies for the days in each WT is depicted in Fig. 6a. WT1 and WT2 exhibit cyclonic anomalies in the Atlantic, typically associated to the development of cold fronts to the east of the cyclonic systems (Fig. 6a). Moreover, WT2 demonstrates a more intense

Table 3 Grouping of jet parameters and their associated central parameter according to the PAM algorithm

	Central parameters	Cluster
1	*lat.STJ*	*lat.STJ, latn.STJ, lats.STJ, lon.pac.STJ, lat.pac.STJ, lon.atl.STJ, lat.atl.STJ, ext.lon.atl.STJ, ext.lon.atl.PFJ*
2	*shar.STJ*	*int.STJ, shar.STJ, int.pac.STJ, int.atl.STJ, hei.pac.STJ, tilt.pac.PFJ*
3	*dep.STJ*	*dep.STJ, ext.lon.pac.STJ, tilt.pac.STJ, tilt.atl.STJ, tilt.atl.PFJ*
4	*branches.STJ*	*branches.STJ, hei.atl.STJ*
5	*lat.PFJ*	*lat.PFJ, latn.PFJ, lats.PFJ, lat.pac.PFJ, lat.atl.PFJ, hei.pac.PFJ, hei.atl.PFJ*
6	*int.PFJ*	*int.PFJ, shar.PFJ, dep.PFJ, int.atl.PFJ*
7	*ext.lon.pac.PFJ*	*branches.PFJ, lon.pac.PFJ, ext.lon.pac.PFJ, int.pac.PFJ, lon.atl.PFJ*

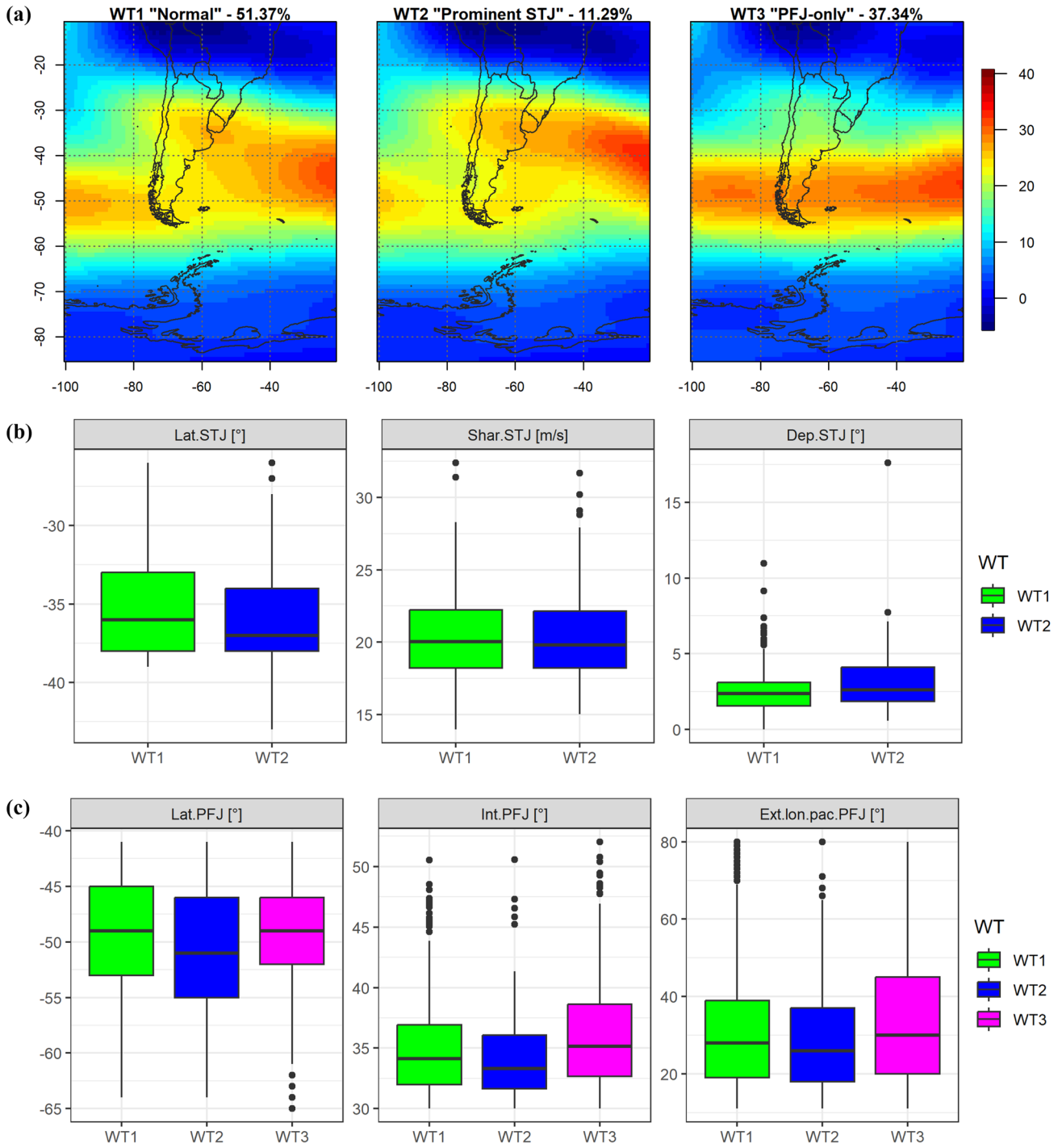

Fig. 4 Synoptic Weather Types (WT) of the weighted vertically averaged zonal wind between 400 and 100 hPa and percentage of days corresponding to each group [m/s] (**a**). Boxplots of the STJ medoid parameters for the WTs with the jet present (**b**). Boxplots of the PFJ medoid parameters (**c**). The boxplots show the median and the first and third quartiles, their whiskers extend from the hinge up to a distance of 1,5 * IQR (where IQR is the interquartile range), and the data beyond the end of the whiskers are the outlier points and are plotted individually

configuration due to the presence of anticyclonic anomalies in the Antarctic Peninsula region, which channels the southerly flow and results in larger cold anomalies (Fig. 6a–c). This circulation pattern leads to the irruption of cold air in the southern region of SA east of the Andes (Fig. 6b, c). The occurrence of strong and long-lived cold surges

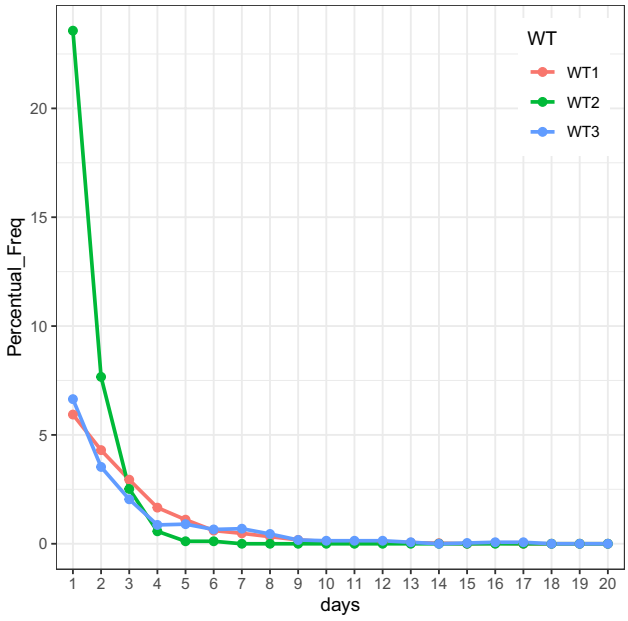

Fig. 5 Percentage frequency of the persistence of each synoptic WT of the weighted vertically averaged zonal wind between 400 and 100 hPa

Table 4 Percentage of permanence and transition between the *synoptic WT of the weighted vertically averaged zonal wind between 400 and 100 hPa*

	From WT		
To WT	1	2	3
1	65%	59%	30%
2	13%	31%	3%
3	22%	9%	67%

in subtropical SA is closely related to the presence of an upper-level jet entrance (Garreaud 2000). This jet entrance induces an ageostrophic direct circulation that reinforces the near-surface southerly flow and leads to an intensification of the cold air incursion (Marengo et al. 1997; Hamilton and Tarifa, 1978; Garreaud 2000; Lanfredi and de Camargo 2018). Regions other than southern SA east of the Andes show significant temperature and precipitation anomalies: in southern Chile, cyclonic anomalies in the Pacific Ocean in WT2 trigger increased convection and wet conditions (Fig. 6a, d, e); conversely, inhibition of convection in northern and eastern Brazil leads to drought conditions and the occurrence of warm maximum temperature anomalies due to soil moisture-atmosphere feedback (Fig. 6b, d, e). This region has a strong soil moisture-atmosphere coupling throughout the year, which has been shown to partially drive temperature variability (Menéndez et al. 2019).

Unlike the other two patterns, WT3 displays anticyclonic anomalies in the South Atlantic Ocean and cyclonic anomalies in the north of SA (Fig. 6a), which could lead to atmospheric blocking in the region (Rodrigues and Woollings 2017). The cyclonic anomalies in northern SA, with a center over southern Brazil, promote convergence and enhanced convection and precipitation (Fig. 6b, d, e). Summer rainfall in tropical and subtropical SA is associated with two convergence zones: the Intertropical Convergence Zone (ITCZ) and the South Atlantic Convergence Zone (SACZ), respectively. Both convergence zones may benefit from the cyclonic conditions observed during this WT3 and show increased activity. The ITZC plays an essential role in the northern tropical SA climate (Vasconcellos et al. 2020). In summer, the southward migration of the ITCZ triggers the rainy season in northeastern SA (Michot et al. 2018). In subtropical SA, SACZ enhancement promotes increased precipitation in Brazil (Carvalho et al. 2004; Gan et al. 2004; Vera et al. 2006; da Silva and de Carvalho 2007; Vasconcelos Junior et al. 2018; Fialho et al. 2023; Pezzi et al. 2023). The SACZ is commonly defined as an extended convective band that typically originates from the Amazon basin, stretches towards the southeast of Brazil, and protrudes into the southeastern subtropical Atlantic Ocean (Kodama 1992, 1993; Carvalho et al. 2002, 2004). Several previous studies have observed that the SACZ induces a dipolar pattern of precipitation anomalies (Casarin and Kousky 1986; Kousky 1988; Kayano and Kousky 1996; Nogués-Paegle and Mo 1997; Herdies 2002; DÍaz and Aceituno 2003; Silva and Berbery 2006; Marengo et al. 2012). The compensatory subsidence branch is located in southeastern SA (Cerne and Vera 2011), resulting in warm anomalies in the region due to clear skies and adiabatic warming (Fig. 6b, c, e). On the other hand, the presence of an anticyclonic center in the South Atlantic Ocean may contribute to warm advection over central Argentina and clear skies over Patagonia.

3.3 3.3 Modulation of the ENSO signal

ENSO exerts a significant influence on the climate patterns of SA, leading to pronounced variations in rainfall, temperature, and atmospheric circulation across the region. Due to this significant impact, we have undertaken an examination of the modulation of ENSO on the WTs obtained in the preceding sections. First, we estimate the frequency of occurrence of each zonal wind pattern (Fig. 4) based on the ENSO phase (Fig. 7). WT1 displays nearly equal probabilities across all ENSO phases, suggesting its independence from ENSO conditions. In contrast, WT2, characterized by a prominent STJ, exhibits a higher probability during the El Niño phase, indicating a potential link between the two. Furthermore, approximately 40% of the days featuring WT3, solely characterized by the PFJ, occur during the La Niña phase. Zooming out to the seasonal scale, we observe that the El Niño phase is associated with a strengthening of the STJ and a deceleration of the PFJ (Fig. S5). This observed correlation aligns with the

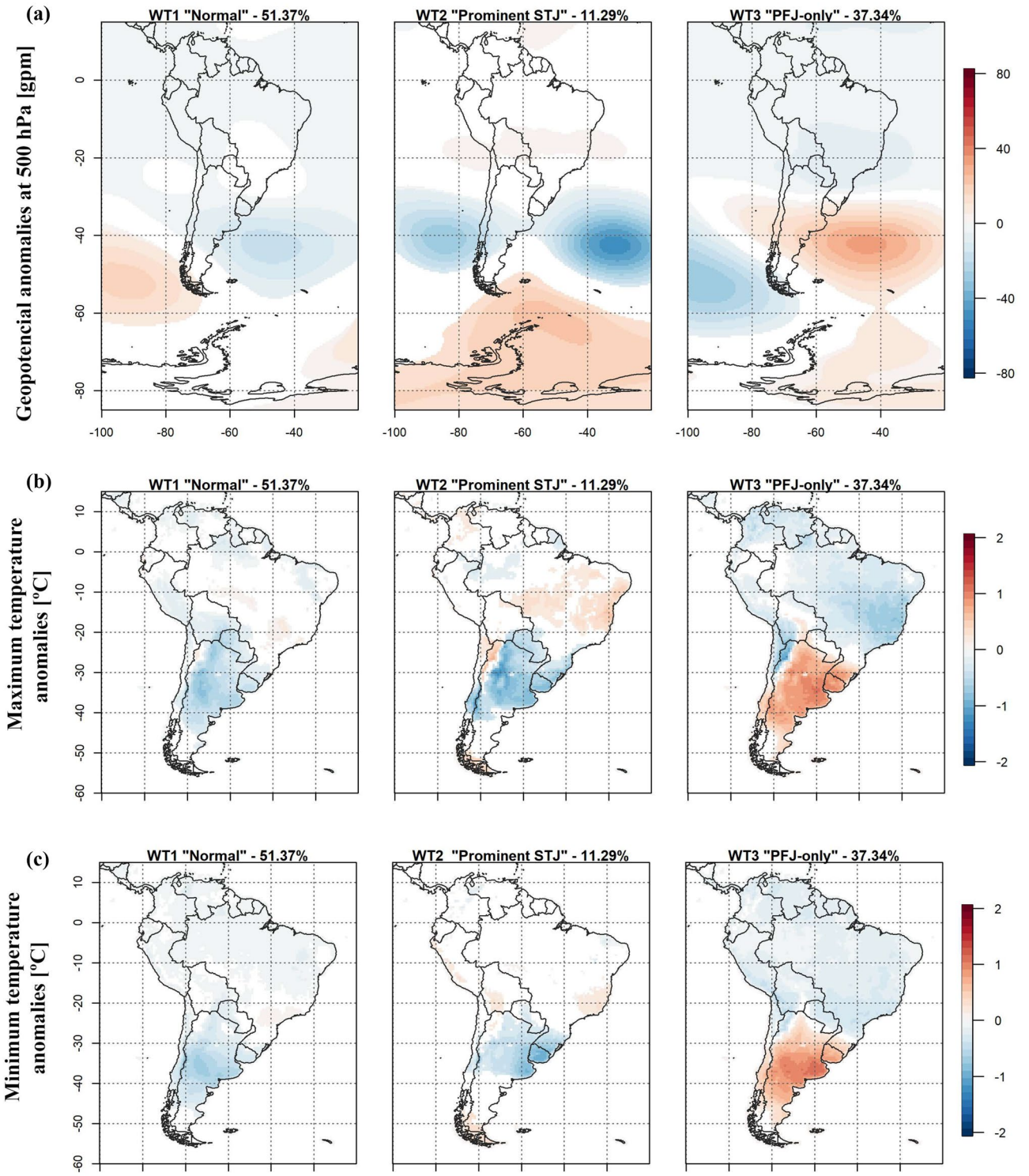

Fig. 6 Composites of the anomalies of: geopotential height at 500 hPa [gpm] (**a**), maximum temperature [ºC] (**b**), minimum temperature [ºC] (**c**), precipitation [mm/day] (**d**), and OLR [W m^{-2}] (**e**) for each of the synoptic patterns obtained from the weighted vertically averaged zonal wind between 400 and 100 hPa. Only anomalies significantly different from zero according to a t-test with a 95% confidence level are shown

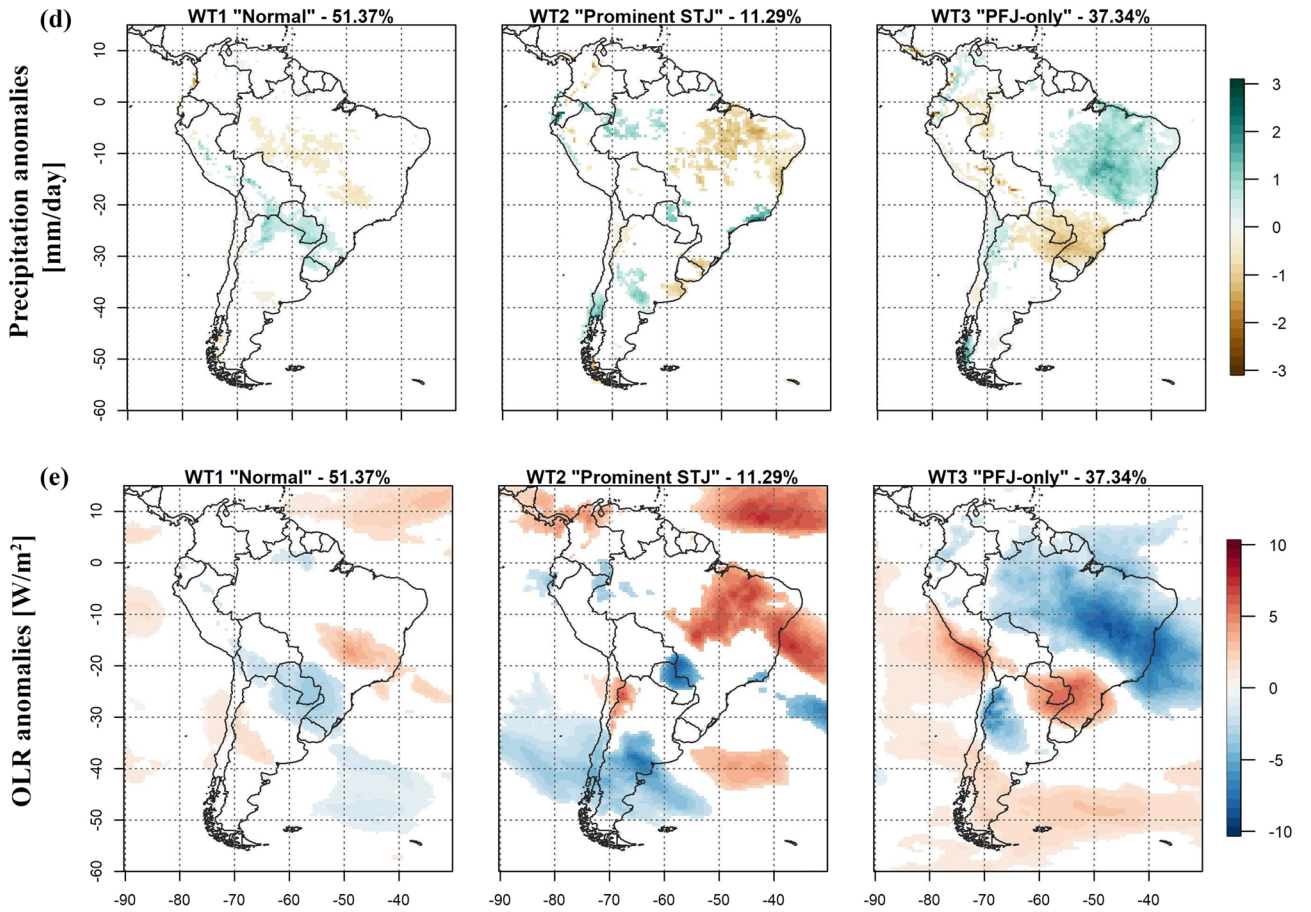

Fig. 6 (continued)

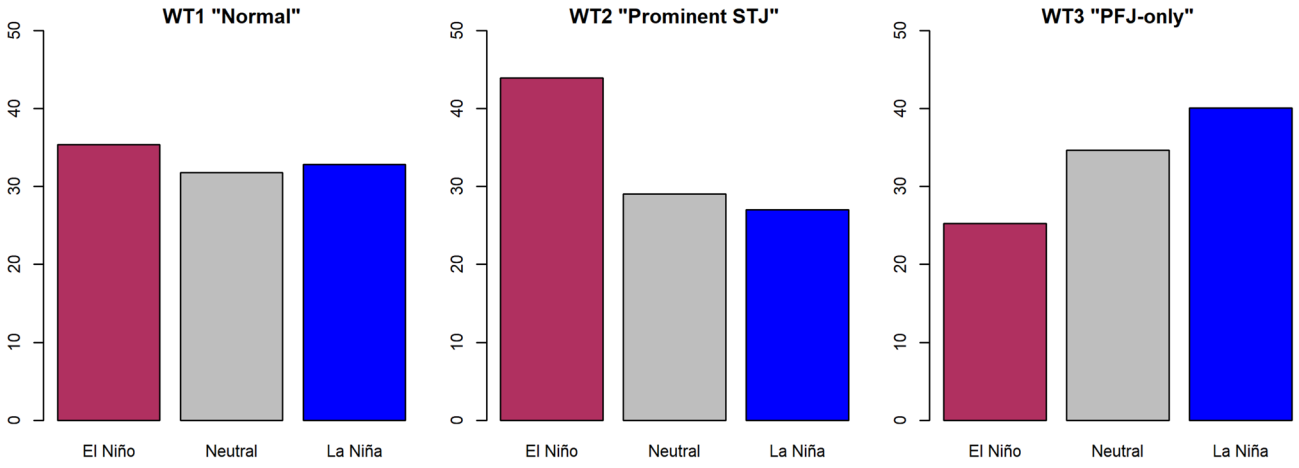

Fig. 7 Frequency of occurrence of each of the synoptic WT according to ENSO phase

frequencies of occurrence obtained for each of the zonal wind patterns, further supporting the consistency between the ENSO phases and the respective zonal wind behaviors.

The resemblance between the expected climatological patterns of temperature and precipitation anomalies for the El Niño and La Niña phases (Fig. S6) and those

derived for these variables within WT2 and WT3 (Fig. 6), respectively, prompted us to investigate whether the zonal wind configuration significantly contributes to these anomalies, or if they predominantly arise as a response to the ENSO signal across the region. For this purpose, we generated composites of meteorological variables by classifying days according to their zonal wind WT and ENSO phase. We then evaluated whether the composites obtained from these variables significantly differed from the ENSO climatology (Fig S5). Figure 8 presents these differences for the maximum temperature anomalies. In WT1 and during El Niño, the zonal wind pattern intensifies the cold anomalies typically expected during this ENSO phase in central and northern Argentina. Simultaneously, it promotes warm conditions in eastern Brazil through the inhibition of convection. During the ENSO neutral phase, significant differences are obtained over an even larger area. In the case of La Niña, anomalies of the opposite sign to those expected according to the ENSO climatology are recorded in central Argentina and Uruguay. However, no significant differences are observed in the rest of the regions.

When El Niño coincides with WT2, it reinforces the effects of the STJ, resulting in unusually cold conditions in Argentina and Uruguay. During the ENSO neutral phase, the prominent STJ primarily affects central and northeastern Brazil. In this configuration, warm anomalies associated with WT2 prevail due to the suppression of precipitation (Fig. S7). Lastly, under La Niña conditions in conjunction with WT2, a distinct signal emerges where anomalies contrary to ENSO climatology are observed in central Chile and Argentina, and central-eastern Brazil. This deviation from expected patterns is primarily influenced by the pronounced jet stream associated with WT2.

Composites of the maximum temperature anomalies under the PFJ-only pattern (WT3) and discrimination based on the ENSO phase reveal that the synoptic signal is dominant over the low-frequency variability signal. This implies that the absence of the STJ leads to warm (cold) conditions in southern South America (Brazil), irrespective of the ENSO phase, because of the presence of anticyclonic anomalies in the Atlantic and cyclonic anomalies over Brazil. Similar results are found for minimum temperature anomalies (not shown). Regarding precipitation, significant results are observed only in localized areas of the continent (Fig. S7), mainly in central-eastern Brazil and Paraguay under WT2 and WT3. It is worth noting that in the northwest region of South America, ENSO tends to be the primary driver of temperature and precipitation anomalies. In this area, the configuration of zonal wind at upper levels does not significantly contribute to these anomalies.

3.4 3.4 Influence of the upper-level jets on warm spells

The remarkable impact of zonal wind patterns on maximum temperature has motivated us to explore their influence on the warm extremes of this variable. The analysis of the climatology of the WS occurrence probability in SA reveals that the southeastern region of the continent and Colombia exhibit the highest likelihood of experiencing WS. In these regions, approximately 10% of summer days are classified as belonging to a WS (Fig. S8). Conversely, the central-western region of Brazil demonstrates a lower probability of encountering such extremely warm events.

To quantify the relationship between the occurrence of a day in a WS and the upper-level zonal wind patterns, we estimate the percentage increase in the conditional probability of WS occurrence for each of the three WTs with respect to the WS climatology (Fig. 9). The WT1 significantly decreases the probability of WS occurrence by approximately 50% compared to the climatology in central Argentina. In contrast, in the central-eastern region of Brazil, it contributes to an increase in the WS probability by around 45%. For the other two patterns, the effects are even more intense. The conditional probability of a WS occurrence in southern SA is consistent with the findings mentioned earlier regarding maximum temperature anomalies. The occurrence of WT2 inhibits the possibility of WS occurrence in a significant portion of southern SA. However, in regions such as northern SA, northern Chile, the Peruvian coast, parts of Bolivia, and Brazil, the occurrence of this pattern more than doubles the probability of WS compared to the climatological average. Identifying the occurrence of this specific zonal wind pattern yields valuable insights into temperature extremes across the region. The absence of the STJ (WT3) almost doubles the probability of WS in southern SA, while resulting in a reduction of about 75% of this probability in tropical SA.

Continuing from our previous analysis, it is worth exploring how these results are influenced by the various phases of the ENSO. Firstly, we examine the climatological probability of the occurrence of WS in each ENSO phase (Fig. S9). As expected, the interaction between soil and atmosphere plays a crucial role, and we observe that regions where drought conditions are most likely in each ENSO phase (Fig. S6) tend to have the highest probabilities of experiencing WS (Fig. S9). These regions are the northern SA during the El Niño phase and the southeastern SA during La Niña. It is important to note that in northern SA during the La Niña phase, no WS occurs because wet conditions are favored.

Subsequently, we examine how the climatological probability of WS occurrence during different ENSO phases is modified by considering the zonal wind pattern at upper levels (Fig. 10). As observed in the previous section regarding maximum temperature anomalies, the synoptic WT signal

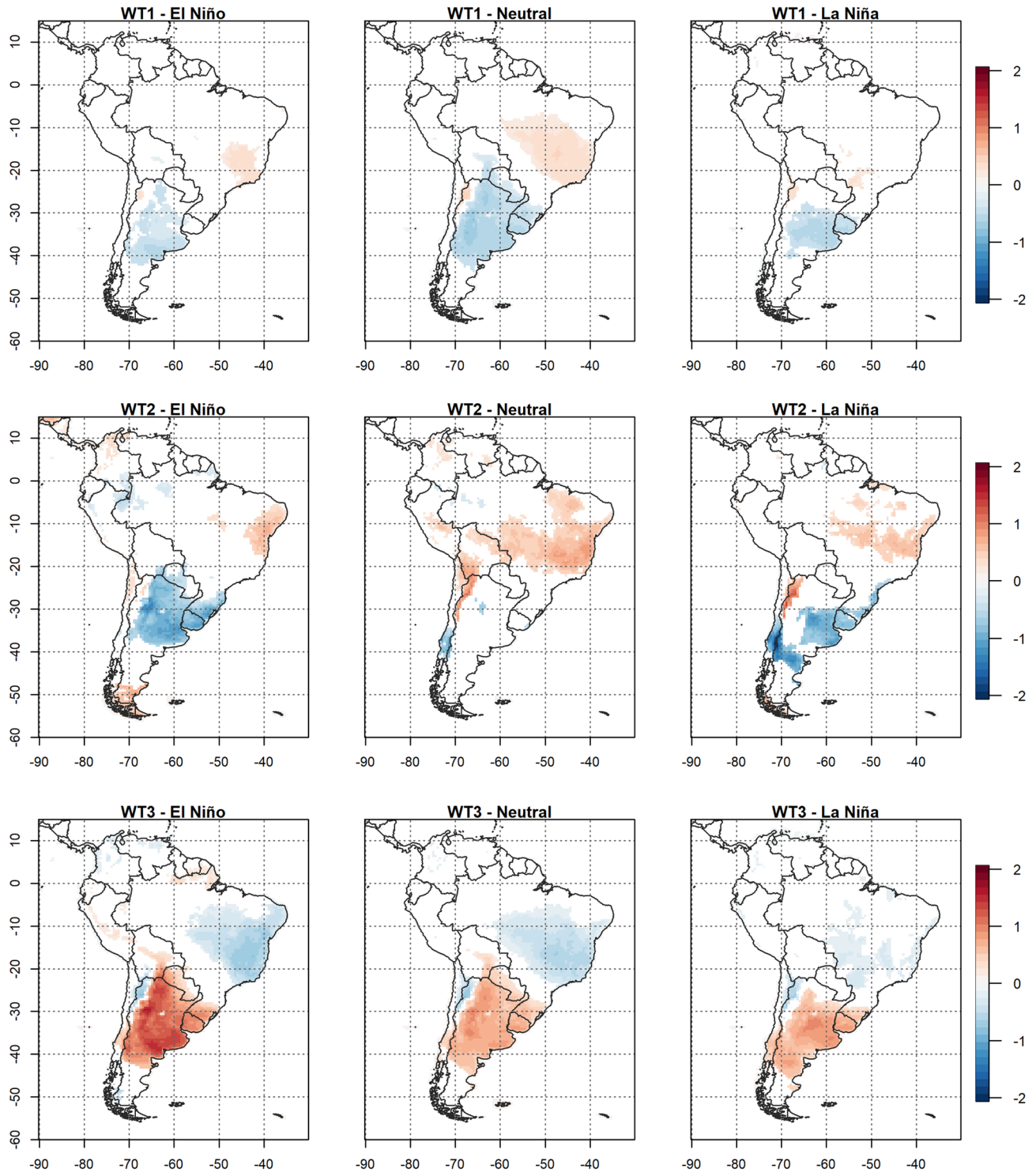

Fig. 8 Mean difference between the maximum temperature anomalies obtained for each synoptic pattern and ENSO phase and the expected for this variable according to ENSO climatology. Only anomalies significantly different from zero according to a t-test with a 95% confidence level are shown

outweighs the influence of ENSO at the warm extremes, particularly in central and northern Argentina. In this region, the combination of any ENSO phase with WT1 and WT2 results in an average reduction in the probability of WS occurrence compared to the expected frequency based on ENSO climatology. In particular, when a prominent STJ

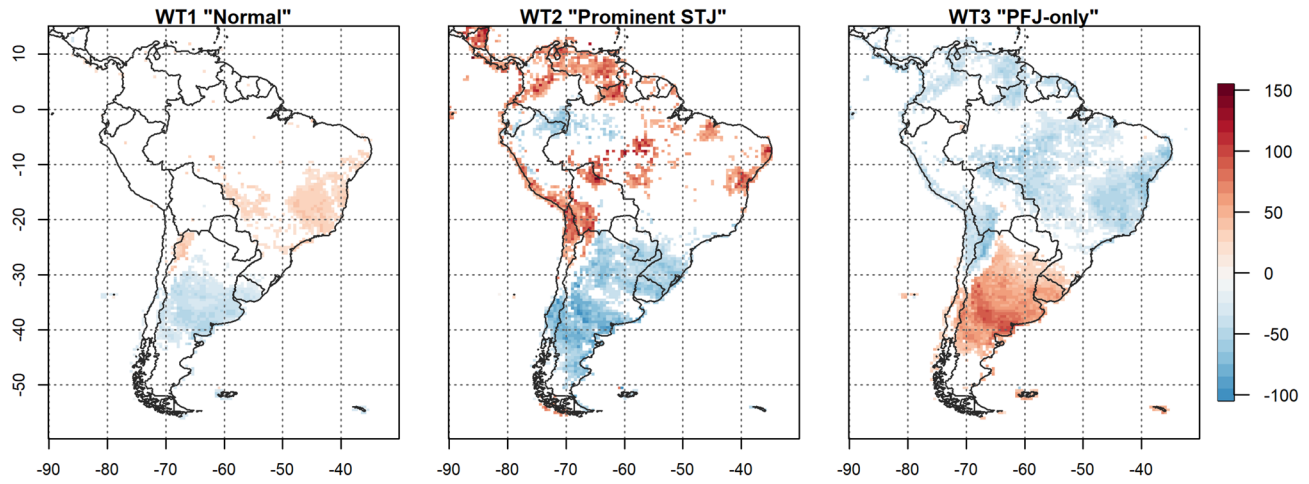

Fig. 9 Percentage increase in the conditional probability of occurrence of a WS for each synoptic pattern respect the probability of WS expected by climatology [%]. Only significant differences according to Z-statistic at 95% confidence level are shown

coincides with the La Niña phase, no instances of WS are observed. In contrast, the PFJ-only pattern, regardless of the ENSO phase, promotes a higher frequency of WS. Notably, in central Argentina, the likelihood of WS is three times higher than expected based on El Niño climatology when this phase is combined with WT3.

4 Discussion

Our study has made substantial advancements in understanding upper-level jets in SA by introducing new parameters that provide valuable insights into their behavior. These parameters uncover novel properties and enhance our ability to interpret and disentangle different aspects of the jet configuration, including temporal and spatial discontinuities during the austral summer. Hemispheric-scale studies have traditionally shown that, on average, only one jet exists in the SH during the austral summer (Nakamura and Shimpo 2004; Gallego et al. 2005). However, our focused investigation on SA has revealed more details. We have observed the presence of the STJ on approximately 60% of summer days in the region. The preferred locations of the STJ are upstream of the Andes Mountain range or over the east coast of the continent, with the latter (Atlantic branch) capable of reaching higher wind speeds. In addition, we have found that the northwest-southeast tilt of the STJ is more frequent, which is consistent with the inclination at the front of the trough (Janach 2015). The PFJ is constantly present during the summer with generally one or two branches. In addition, its latitudinal variability is higher when compared to the more stable STJ latitudes. This difference between the two jets can be attributed to their distinct formation mechanisms (Pena-Ortiz et al. 2013; Simmons 2022).

We have identified a poleward shift of the PFJ that is consistent with previous studies from different reanalyses (Pena-Ortiz et al. 2013; Manney and Hegglin 2018; WMO 2018; Waugh et al. 2020). This general poleward movement of midlatitude jet streams is consistent with the expansion of the tropical circulation (Lucas et al. 2014) and is related to the annular modes of variability and ozone depletion (Son et al. 2010; Arblaster et al. 2011; Polvani et al. 2011; McLandress et al. 2011; Banerjee et al. 2020). The acceleration of the PFJ and the increase in height are also consistent across studies (Pena-Ortiz et al. 2013; Manney and Hegglin 2018). However, our analysis focused on the jet branches allowed us to uncover differences between the ocean basins. We observed that the acceleration of the PFJ in the Atlantic basin is approximately twice as high as that derived from zonal mean analysis. Conversely, no significant changes are observed in the acceleration of the PFJ in the Pacific basin. On the other hand, the poleward shift of the PFJ is found to be significant only in the Pacific basin. This difference between the two basins results in an increase in the latitudinal spread of the PFJ and a more pronounced elevation in the Atlantic branch of the PFJ.

While employing a wide range of parameters enables us to provide a comprehensive characterization of the jets, it is important to consider that many of them are not independent of each other. Hence, it is possible to identify a subset of parameters to facilitate a more concise analysis of the jets. Traditionally, jet investigations focus on analyzing the latitudinal position and the maximum wind speed of the jets (Blackmon et al. 1977; Kidson 1999; Bracegirdle et al. 2018, 2020; Zolotov et al. 2018). However, our study reveals that for a more complete description of STJ during the austral summer in SA, it is relevant to consider not only its latitude and intensity but also the latitudinal

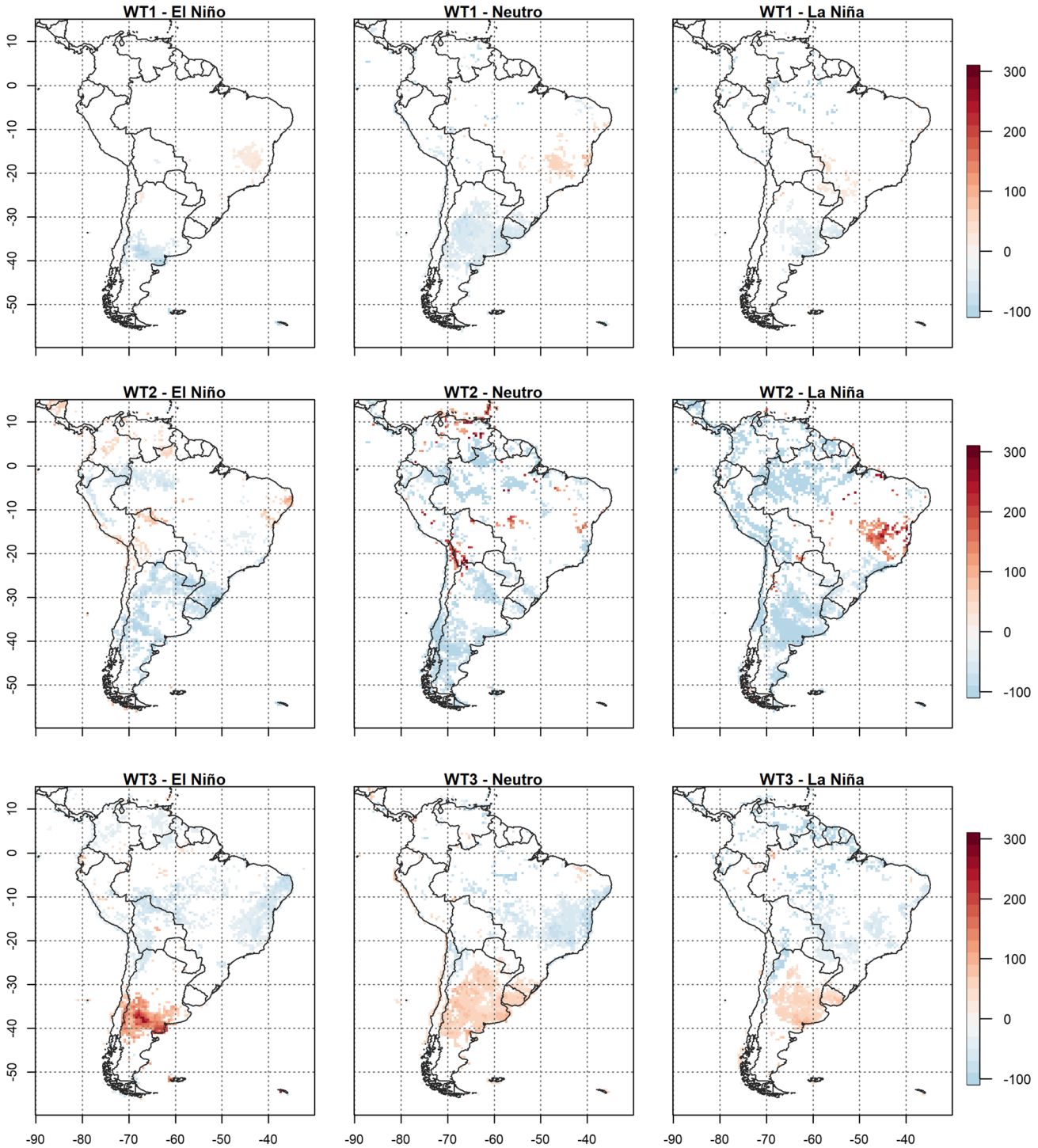

Fig. 10 Percentage increase in the conditional probability of occurrence of a WS for each synoptic pattern respect the probability of WS expected by ENSO climatology [%]. Only significant differences according to Z-statistic at 95% confidence level are shown

fluctuations and temporal discontinuity. On the other hand, the PFJ only requires three parameters—latitude, intensity, and longitudinal extent of the Pacific branch—since it consistently manifests during the summer. The *ext.lon.pac. PFJ* is a distinct characteristic that exhibits considerable variability and is not adequately represented by the other two parameters.

From this new description of the jets, we can obtain three WTs of the zonal wind at upper atmospheric levels, which are characteristic of summer days. The first pattern

represents normal jet conditions during the summer as it groups approximately 50% of the days and is similar to the climatological field. The second pattern presents a prominent STJ over central Argentina and the Atlantic Ocean with latitudinal fluctuations. Finally, the third pattern groups the days where only the PFJ is present. These patterns are obtained from a set of parameters that characterize the jets and from clustering techniques and they provide physically based partition that is not obtained with classical methods such as Empirical Orthogonal Functions (EOFs). By utilizing jet parameters and employing the PAM clustering technique, we successfully obtained meaningful patterns that are easily interpretable. Additionally, this approach enabled us to classify each of the summer days into specific clusters, facilitating composite analysis of multiple meteorological variables. We performed an exploratory analysis of the patterns obtained with EOF of the upper-level zonal wind anomalies (Fig. S10). In contrast with our results, we observed that none of the EOFs explain a large percentage of variance and the patterns are difficult to interpret. This is not surprising, recent research has highlighted that EOF analysis can sometimes yield patterns that lack physical significance (Fulton and Hegerl 2021). Dommenget and Latif (2002) find that EOF is susceptible to identifying dipoles even when they do not exist, and Monahan et al. (2009) show that the principal components do not correspond to distinct dynamical modes. Furthermore, in situations where true modes exist but are nonorthogonal to each other, even the first EOF is unable to capture a genuine underlying mode.

In this study, we have examined the connection between WTs and atmospheric circulation, as well as their impact on temperature and precipitation patterns over SA. To ensure greater robustness of our findings, we have replicated the composite analyses of minimum and maximum temperatures, as well as precipitation, using both the ERA5 reanalysis and the CPC observational dataset. The results obtained from both datasets exhibit a high degree of similarity, highlighting a prevalence of cold anomalies in southern SA and warm anomalies in eastern Brazil when the STJ is present (not shown). Conversely, an opposite pattern emerges when the STJ is absent. By employing these two distinct datasets, we enhance the reliability and validity of our results.

Due to the significant influence of ENSO on the climate of SA, we conducted a thorough exploration of the sensitivity of our results to the different ENSO phases. ENSO impacts manifest through the anomalous circulation of the Walker cell, descending from its typical position and affecting the tropical region. Additionally, extratropical effects are observed through Rossby wave trains via the Pacific-South American pattern (Cai et al. 2020; Reboita et al. 2021; and references therein). Our study revealed that ENSO plays a role in modulating the frequency of zonal wind patterns, particularly with a higher occurrence of the PFJ-only pattern during the La Niña phase and a prominent STJ during El Niño events. However, when examining the daily temperature response, it becomes evident that synoptic jet conditions dominate over the ENSO phase across much of SA. The exception to this pattern is observed in the northwestern region of the continent, where the dominant signal is attributed to ENSO.

The impacts of ENSO, through its teleconnections, are subject to the influence of numerous factors, resulting in high event-to-event variability. Previous studies have revealed nonstationary behavior in the occurrence of warm ENSO events over the past few centuries (Garcia-Herrera et al. 2008), as well as in the strengths of Australasian teleconnections (Mullan 1995; Nicholls et al. 1996; Verdon and Franks 2006; Risbey et al. 2009; Gallant et al. 2013). This non-stationarity arises partially from changes in the large-scale state of the coupled atmosphere–ocean system, leading to fluctuations in the amplitude and spatial patterns of ENSO-related sea surface temperature anomalies (Cai et al. 2020). But in addition, other studies have suggested that teleconnections can be modified by the effects of synoptic-scale weather systems (Meyers et al. 2007; Fogt et al. 2011). Our study shows that the synoptic variability of the jet stream can modulate the ENSO response, primarily affecting temperature patterns in southern SA and the precipitation in localized regions. Moreover, we find that the synoptic weather patterns of the zonal wind exert a notable influence on the frequency of warm extremes in maximum temperature. This influence significantly alters the probability of occurrence of these extremes compared to the climatological probability in each ENSO phase and explains part of the nonstationary ENSO teleconnections.

5 Summary and conclusions

In this study, we aim to investigate the influence of upper-level jets on temperature and precipitation patterns in SA during the austral summer, while also accounting for the ENSO impact. To achieve this, we utilize the ERA5 reanalysis dataset from 1979 to 2022. Through a comprehensive daily characterization of jet streams using multiple parameters, we obtain synoptic weather patterns that capture the zonal wind dynamics. By employing composites of multiple meteorological variables, we delve into the associated atmospheric circulation patterns and examine the influence of different jet stream configurations on warm spells. The main conclusions are summarized as follows:

- *Analysis of jet parameters:* The parameters introduced in this study for jet characterization provide us with the means to quantify the daily variability of the STJ during summer, as it is absent in approximately 40% of the

days. Furthermore, these parameters have proven valuable in capturing the spatial discontinuities of the jets over SA, which are often influenced by the presence of the Andes Mountain range. In particular, we note that the maximum intensity of the Pacific branch of the jets tends to be located just west of the mountain range, especially for the STJ. Additionally, we have observed that the STJ tends to display a preferential inclination in a northwest-to-southeast (NW–SE) direction. Regarding the PFJ, it maintains a persistent presence and displays greater intensities, as well as a broader latitudinal range, in comparison to the STJ.

- *Long-term changes in jet parameters:* Examining the trends of these newly defined parameters over the period 1979–2022 enables us to discern notable distinctions between the ocean basins, which would otherwise remain unnoticed if only zonal averages of the jet properties are analyzed. Significant long-term changes have been observed in the PFJ, revealing a poleward shift of its branch in the Pacific basin, an acceleration of its Atlantic branch, and an elevation of both branches (with a greater rise observed in the Atlantic branch). Consequently, these changes have led to an increase in the latitudinal deviation of the jet, indicating a widening spread of its position.
- *A new characterization of the jet streams:* To obtain a concise description of the jet streams, and considering that many of the defined parameters exhibit interdependence, we identify a subset of relevant parameters. Our findings indicate that for a comprehensive characterization of the summer jets over SA, it is insufficient to solely rely on information about the latitude and intensity of the jets. The departure and branch number of the STJ and the longitudinal extent of the Pacific branch of the PFJ are also necessary for a thorough understanding. The requirement for four parameters to describe the STJ and three parameters for the PFJ arises from the inherent variability of the STJ, which is not consistently present on all summer days.
- *Weather Types based on jet configuration:* Synoptic weather patterns of the upper-level zonal wind are obtained from this new characterization of the jets. We find that the summer days can be classified into three WTs: normal conditions, prominent STJ, and PFJ-only. In the latter, anticyclonic anomalies are observed in the South Atlantic Ocean and increased convection is favored over Brazil. Consequently, this leads to clear skies and warm advection over southern SA and increased precipitation over Brazil with cold anomalies. In addition, we observe that this WT has the longest persistence, while prominent STJ patterns are of shorter duration and tend to evolve to normal conditions.
- *Role of ENSO:* We find that the temperature anomalies in southern SA and east-central Brazil associated with WTs are not dependent on the ENSO phase. In other words, the dominant factor influencing these anomalies is the synoptic signal, rather than the low-frequency variability signal. However, we observe that ENSO does influence the frequency of occurrence of these patterns. During La Niña events, the PFJ-only pattern tends to be more prevalent, whereas during El Niño, a prominent STJ pattern is observed more frequently.
- *Warm spells occurrence:* The occurrence of warm maximum temperature extremes is also influenced by jet patterns in many regions of SA, including most of Argentina, Uruguay, central and northern Chile, and eastern Brazil. These regions show significant changes in the climatological occurrence probability of these events according to the jet configuration. Even a complete inhibition of WS is observed in central Argentina due to the presence of the prominent STJ.

The climate of SA is influenced by several teleconnections operating on various time scales (Reboita et al. 2021). This study focuses on analyzing the influence of ENSO on upper-level zonal wind patterns, as ENSO represents one of the primary modes of climate variability with significant impacts across the entire continent. However, other modes of variability, ozone hole, greenhouse gases, and stratospheric sudden warmings can influence the jet configurations (Thompson et al. 2011; Gerber and Son 2014; Young et al. 2014; Haase et al. 2020; Domeisen and Butler 2020). The new jet stream characterization and WTs obtained in this study have the potential to serve as a valuable tool for advancing future research in these fields within the unique context of the SA region. Understanding the relationship between the identified synoptic patterns and these processes can provide valuable insights into how the atmosphere responds to large-scale climate variability, and how these patterns may change under future climate scenarios.

Supplementary Information The online version contains supplementary material available at https://doi.org/10.1007/s00382-023-06955-9.

Acknowledgements This work was supported by the SAFETE project, which has received funding from the European Union's Horizon 2020 research and innovation program under the Marie Skłodowska-Curie grant agreement No 847635 (UNA4CAREER).

Author contributions All authors contributed to the study conception, analysis, and design. Material preparation and data collection were performed by Soledad Collazo. The first draft of the manuscript was written by Soledad Collazo and all authors commented on previous versions of the manuscript. All authors read and approved the final manuscript.

Funding Open Access funding provided thanks to the CRUE-CSIC agreement with Springer Nature. This work was supported by the

European Union's Horizon 2020 research and innovation program under the Marie Skłodowska-Curie grant agreement No 847635 (UNA4CAREER) through the SAFETE project (code 4230420).

Data availability Datasets used in this study is publicly accessible online via the following links: ERA5: https://climate.copernicus.eu/climate-reanalysis. CPC: https://psl.noaa.gov/data/gridded/data.cpc.globalprecip.html, https://psl.noaa.gov/data/gridded/data.cpc.globaltemp.html. ONI index: https://origin.cpc.ncep.noaa.gov/products/analysis_monitoring/ensostuff/ONI_v5.php.

Declarations

Conflict of interest The authors have no relevant financial or non-financial interests to disclose.

References

Arblaster JM, Meehl GA, Karoly DJ (2011) Future climate change in the Southern Hemisphere: competing effects of ozone and greenhouse gases. Geophys Res Lett. https://doi.org/10.1029/2010GL045384

Archer CL, Caldeira K (2008) Historical trends in the jet streams. Geophys Res Lett 35:L08803. https://doi.org/10.1029/2008GL033614

Banerjee A, Fyfe JC, Polvani LM et al (2020) A pause in Southern Hemisphere circulation trends due to the Montreal Protocol. Nature 579:544–548. https://doi.org/10.1038/s41586-020-2120-4

Barreiro M (2010) Influence of ENSO and the South Atlantic Ocean on climate predictability over Southeastern South America. Clim Dyn 35:1493–1508. https://doi.org/10.1007/s00382-009-0666-9

Barriopedro D, Ayarzagüena B, García-Burgos M, García-Herrera R (2022) A multi-parametric perspective of the North Atlantic eddy-driven jet. Clim Dyn. https://doi.org/10.1007/s00382-022-06574-w

Barriopedro D, García-Herrera R, Ordóñez C et al (2023) Heat Waves: physical understanding and scientific challenges. Rev Geophys. https://doi.org/10.1029/2022RG000780

Barros VR, Grimm AM, Doyle ME (2002) Relationship between temperature and circulation in southeastern South America and its Influence from El Niño and La Niña Events. J Meteorol Soc Jpn 80(1):21–32. https://doi.org/10.2151/jmsj.80.21

Bettolli ML, Penalba OC, Vargas WM (2010) Synoptic weather types in the south of South America and their relationship to daily rainfall in the core crop-producing region in Argentina. Aust Meteorol Oceanographic J. 60:37–48. https://doi.org/10.22499/2.6001.004

Blackmon ML, Wallace JM, Lau N-C, Mullen SL (1977) An Observational Study of the Northern Hemisphere Wintertime Circulation. J Atmos Sci 34:1040–1053. https://doi.org/10.1175/1520-0469

Bracegirdle TJ, Hyder P, Holmes CR (2018) CMIP5 diversity in southern westerly jet projections related to historical sea ice area: strong link to strengthening and weak link to shift. J Clim 31:195–211. https://doi.org/10.1175/JCLI-D-17-0320.1

Bracegirdle TJ, Holmes CR, Hosking JS et al (2020) Improvements in Circumpolar Southern Hemisphere Extratropical Atmospheric Circulation in CMIP6 Compared to CMIP5. Earth Space Sci. https://doi.org/10.1029/2019EA001065

Bruick ZS, Rasmussen KL, Rowe AK, McMurdie LA (2019) Characteristics of intense convection in subtropical South America as influenced by El Niño–Southern oscillation. Mon Wea Rev 147:1947–1966. https://doi.org/10.1175/MWR-D-18-0342.1

Cai W, McPhaden MJ, Grimm AM et al (2020) Climate impacts of the El Niño-Southern Oscillation on South America. Nat Rev Earth Environ 1:215–231. https://doi.org/10.1038/s43017-020-0040-3

Calinski T, Harabasz J (1974) A dendrite method for cluster analysis. Commun Stat Theory Methods 3:1–27. https://doi.org/10.1080/03610927408827101

Carvalho LMV, Jones C, Liebmann B (2002) Extreme precipitation events in southeastern south america and large-scale convective patterns in the South Atlantic Convergence Zone. J Clim 15:2377–2394. https://doi.org/10.1175/1520-0442

Carvalho LMV, Jones C, Liebmann B (2004) The South atlantic convergence zone: intensity, form, persistence, and relationships with intraseasonal to interannual activity and extreme rainfall. J Clim 17:88–108. https://doi.org/10.1175/1520-0442

Casarin DP, Kousky VE (1986) Precipitation anomalies in Southern Brazil and related changes in the atmospheric circulation. Revista Brasileira De Meteorologia 1:83–90

Cattiaux J, Peings Y, Saint-Martin D et al (2016) Sinuosity of midlatitude atmospheric flow in a warming world. Geophys Res Lett 43:8259–8268. https://doi.org/10.1002/2016GL070309

Cerne SB, Vera CS (2011) Influence of the intraseasonal variability on heat waves in subtropical South America. Clim Dyn 36:2265–2277. https://doi.org/10.1007/s00382-010-0812-4

Chen HW, Zhang F, Alley RB (2016) The robustness of Midlatitude weather pattern changes due to arctic sea ice loss. J Clim 29:7831–7849. https://doi.org/10.1175/JCLI-D-16-0167.1

Choudhury D, Nath D, Chen W (2021) The modulation of Indian summer monsoon onset processes during ENSO through equatorward migration of the subtropical jet stream. Clim Dyn 57:141–152. https://doi.org/10.1007/s00382-021-05700-4

Collazo S, Barrucand M, Rusticucci M (2019a) Summer seasonal predictability of warm days in Argentina: statistical model approach. Theor Appl Climatol 138:1853–1876. https://doi.org/10.1007/s00704-019-02933-6

Collazo S, Barrucand M, Rusticucci M (2019) Variability and predictability of winter cold nights in Argentina. Weather Clim Extrem. 26:100236. https://doi.org/10.1016/j.wace.2019.100236

da Silva AE, de Carvalho LMV (2007) Large-scale index for South America Monsoon (LISAM). Atmospheric Sci Lett 8:51–57. https://doi.org/10.1002/asl.150

Di Capua G, Coumou D (2016) Changes in meandering of the Northern Hemisphere circulation. Environ Res. Lett. 11:094028. https://doi.org/10.1088/1748-9326/11/9/094028

DI Domeisen V, Butler AH (2020) Stratospheric drivers of extreme events at the Earth's surface. Commun Earth Environ 1:59. https://doi.org/10.1038/s43247-020-00060-z

DÍaz A, Aceituno P (2003) Atmospheric circulation anomalies during episodes of enhanced and reduced convective cloudiness over Uruguay. J Clim 16:3171–3185. https://doi.org/10.1175/1520-0442

Ding Q, Steig EJ, Battisti DS, Wallace JM (2012) Influence of the Tropics on the Southern Annular Mode. J Clim 25:6330–6348. https://doi.org/10.1175/JCLI-D-11-00523.1

Dommenget D, Latif M (2002) A Cautionary Note on the Interpretation of EOFs. J Clim 15:216–225. https://doi.org/10.1175/1520-0442

Fatmasari D (2021) The regional hadley cells response to the sea surface temperature distribution across the indo-pacific ocean. IOP Conf Ser Earth Environ Sci 893:012008. https://doi.org/10.1088/1755-1315/893/1/012008

Fialho WMB, Carvalho LMV, Gan MA, Veiga SF (2023) Mechanisms controlling persistent South Atlantic Convergence Zone events on intraseasonal timescales. Theor Appl Climatol 152:75–96. https://doi.org/10.1007/s00704-023-04375-7

Fogt RL, Bromwich DH, Hines KM (2011) Understanding the SAM influence on the South Pacific ENSO teleconnection. Clim Dyn 36:1555–1576. https://doi.org/10.1007/s00382-010-0905-0

Fulton DJ, Hegerl GC (2021) Testing methods of pattern extraction for climate data using synthetic modes. J Clim 34:7645–7660. https://doi.org/10.1175/JCLI-D-20-0871.1

Gallant AJE, Phipps SJ, Karoly DJ et al (2013) Nonstationary Australasian teleconnections and implications for paleoclimate reconstructions. J Clim 26:8827–8849. https://doi.org/10.1175/JCLI-D-12-00338.1

Gallego D, Ribera P, Garcia-Herrera R et al (2005) A new look for the Southern Hemisphere jet stream. Clim Dyn 24:607–621. https://doi.org/10.1007/s00382-005-0006-7

Gan MA, Kousky VE, Ropelewski CF (2004) The South America Monsoon Circulation and its relationship to rainfall over West-Central Brazil. J Clim 17:47–66. https://doi.org/10.1175/1520-0442

Garcia-Herrera R, Barriopedro D, Hernández E et al (2008) A Chronology of El Niño Events from Primary Documentary Sources in Northern Peru*. J Clim 21:1948–1962. https://doi.org/10.1175/2007JCLI1830.1

Garreaud RD (2000) Cold air incursions over subtropical South America: mean structure and dynamics. Mon Weather Rev 128:2544–2559. https://doi.org/10.1175/1520-0493

Garreaud RD (2009) The Andes climate and weather. Adv Geosci 22:3–11. https://doi.org/10.5194/adgeo-22-3-2009

Gerber EP, Son S-W (2014) Quantifying the summertime response of the Austral Jet stream and hadley cell to stratospheric ozone and greenhouse gases. J Clim 27:5538–5559. https://doi.org/10.1175/JCLI-D-13-00539.1

Gower JC (1971) A general coefficient of similarity and some of its properties. Biometrics 27:857. https://doi.org/10.2307/2528823

Grimm AM, Tedeschi RG (2009) ENSO and extreme rainfall events in South America. J Clim 22:1589–1609. https://doi.org/10.1175/2008JCLI2429.1

Haase S, Fricke J, Kruschke T et al (2020) Sensitivity of the Southern Hemisphere circumpolar jet response to Antarctic ozone depletion: prescribed versus interactive chemistry. Atmos Chem Phys 20:14043–14061. https://doi.org/10.5194/acp-20-14043-2020

Hamilton MG, JoséR T (1978) Synoptic aspects of a polar outbreak leading to frost in Tropical Brazil, July 1972. Mon Weather Rev 106:1545–1556. https://doi.org/10.1175/1520-0493

Harnik N, Garfinkel CI, Lachmy O (2016) The influence of jet stream regime on extreme weather events In: dynamics and Predictability of Large-Scale, High-Impact Weather and Climate Events. Cambridge University Press, Cambridge, pp 79–94

Held IM, Hou AY (1980) Nonlinear Axially Symmetric Circulations in a Nearly Inviscid Atmosphere. J Atmos Sci 37:515–533. https://doi.org/10.1175/1520-0469(1980)037%3c0515:NASCIA%3e2.0.CO;2

Held IM, Ting M, Wang H (2002) Northern winter stationary waves: theory and modeling. J Clim 15:2125–2144. https://doi.org/10.1175/1520-0442

Herdies DL (2002) Moisture budget of the bimodal pattern of the summer circulation over South America. J Geophys Res 107:8075. https://doi.org/10.1029/2001JD000997

Hersbach H, Bell B, Berrisford P et al (2020) The ERA5 global reanalysis. Q J R Meteorol Soc 146:1999–2049. https://doi.org/10.1002/qj.3803

Holton JR, Hakim GJ (2013) An introduction to dynamic meteorology, 5th edn. Academic Press, Cambridge, 552 pp. https://doi.org/10.1016/C2009-0-63394-8

Hoskins BJ, Valdes PJ (1990) On the Existence of Storm-Tracks. J Atmos Sci 47:1854–1864. https://doi.org/10.1175/1520-0469

Hoskins BJ, James IN, White GH (1983) The shape, propagation and mean-flow interaction of large-scale weather systems. J Atmos Sci 40:1595–1612. https://doi.org/10.1175/1520-0469

Infante Gil S, Zárate de Lara G (1984) Métodos Estadísticos: un enfoque interdisciplinario. Trillas, Mexico, 643 pp. ISBN: 9789682414220

Janach WE (2015) The physics of jet stream meandering. Adv Syst Sci Appl 15(2):193–201

Kayano MT, Kousky VE (1996) Tropical circulation variability with emphasis on interannual and intraseasonal time scales. Revista Brasilera De Meteorologıa 11:6–17

Kendall MG (1975) Rank correlation methods, 4th edn. Charles Griffin, London

Kidson JW (1999) Principal modes of Southern Hemisphere low-frequency variability obtained from NCEP–NCAR Reanalyses. J Clim 12:2808–2830. https://doi.org/10.1175/1520-0442

Koch P, Wernli H, Davies HC (2006) An event-based jet-stream climatology and typology. Int J Climatol 26:283–301. https://doi.org/10.1002/joc.1255

Kodama Y (1992) Large-scale common features of subtropical precipitation zones (the Baiu frontal zone, the SPCZ, and the SACZ) Part I: characteristics of subtropical frontal zones. J Meteorol Soc Japan Ser II 70:813–836. https://doi.org/10.2151/jmsj1965.70.4_813

Kodama Y-M (1993) Large-scale common features of sub-tropical convergence zones (the Baiu Frontal Zone, the SPCZ, and the SACZ) Part II : conditions of the Circulations for Generating the STCZs. J Meteorol Soc Japan Ser II 71:581–610. https://doi.org/10.2151/jmsj1965.71.5_581

Kousky VE (1988) Pentad outgoing longwave radiation climatology for the South America sector. Revista Brasilera De Meteorologıa 3:217–231

Lanfredi IS, de Camargo R (2018) Classification of extreme cold incursions over South America. Weather Forecast 33:1183–1203. https://doi.org/10.1175/WAF-D-17-0159.1

Lee S, Kim H (2003) The dynamical relationship between subtropical and Eddy-driven jets. J Atmos Sci 60:1490–1503. https://doi.org/10.1175/1520-0469(2003)0602.0.CO;2

Leonard K, Rousseeuw PJ (1990) Finding groups in data. Wiley, Hoboken

Lorenz DJ, DeWeaver ET (2007) Tropopause height and zonal wind response to global warming in the IPCC scenario integrations. J Geophys Res Atmospher. https://doi.org/10.1029/2006JD008087

Lucas C, Timbal B, Nguyen H (2014) The expanding tropics: a critical assessment of the observational and modeling studies. Wiley Interdiscip Rev Clim Change 5:89–112

Mann HB (1945) Nonparametric tests against trend. Econometrica 13:245. https://doi.org/10.2307/1907187

Mann ME, Rahmstorf S, Kornhuber K et al (2017) Influence of anthropogenic climate change on planetary wave resonance and extreme weather events. Sci Rep 7:45242. https://doi.org/10.1038/srep45242

Manney GL, Hegglin MI (2018) Seasonal and regional variations of long-term changes in upper-tropospheric jets from reanalyses. J Clim 31:423–448. https://doi.org/10.1175/JCLI-D-17-0303.1

Marengo J, Cornejo A, Satyamurty P et al (1997) Cold surges in tropical and extratropical South America: the strong event in June 1994. Mon Weather Rev 125:2759–2786. https://doi.org/10.1175/1520-0493

Marengo JA, Tomasella J, Soares WR et al (2012) Extreme climatic events in the Amazon basin. Theor Appl Climatol 107:73–85. https://doi.org/10.1007/s00704-011-0465-1

Martinez DM, Solman SA (2022) Synoptic patterns associated with extreme precipitation events over southeastern South America during spring and summer seasons. Int J Climatol 42:10387–10406. https://doi.org/10.1002/joc.7911

McLandress C, Shepherd TG, Scinocca JF et al (2011) Separating the Dynamical Effects of Climate Change and Ozone Depletion. Part II: Southern Hemisphere Troposphere. J Clim 24:1850–1868. https://doi.org/10.1175/2010JCLI3958.1

Menéndez CG, Giles J, Ruscica R et al (2019) Temperature variability and soil–atmosphere interaction in South America simulated by two regional climate models. Clim Dyn 53:2919–2930. https://doi.org/10.1007/s00382-019-04668-6

Merino RA, Gassmann MI (2022) Wind trends analysis in southern South America from weather station and reanalysis data. Int J Climatol 42:2117–2134. https://doi.org/10.1002/joc.7355

Messori G, Caballero R (2015) On double Rossby wave breaking in the North Atlantic. J Geophys Res: Atmos. https://doi.org/10.1002/2015JD023854

Meyers G, McIntosh P, Pigot L, Pook M (2007) The Years of El Niño, La Niña, and Interactions with the Tropical Indian Ocean. J Clim 20:2872–2880. https://doi.org/10.1175/JCLI4152.1

Michot V, Vila D, Arvor D et al (2018) Performance of TRMM TMPA 3B42 V7 in Replicating Daily Rainfall and Regional Rainfall Regimes in the Amazon Basin (1998–2013). Remote Sens (basel) 10:1879. https://doi.org/10.3390/rs10121879

Milligan GW, Cooper MC (1985) An examination of procedures for determining the number of clusters in a data set. Psychometrika 50:159–179. https://doi.org/10.1007/BF02294245

Monahan AH, Fyfe JC, Ambaum MHP et al (2009) Empirical orthogonal functions: the medium is the message. J Clim 22:6501–6514. https://doi.org/10.1175/2009JCLI3062.1

Montecinos A, Díaz A, Aceituno P (2000) Seasonal diagnostic and predictability of rainfall in subtropical south america based on tropical pacific SST. J Clim 13:746–758. https://doi.org/10.1175/1520-0442

Mullan AB (1995) On the linearity and stability of Southern Oscillation-climate relationships for New Zealand. Int J Climatol 15:1365–1386. https://doi.org/10.1002/joc.3370151205

Nakamura H, Shimpo A (2004) Seasonal variations in the southern hemisphere storm tracks and jet streams as revealed in a reanalysis dataset. J Clim 17:1828–1844. https://doi.org/10.1175/1520-0442

Nicholls N, Lavery B, Frederiksen C et al (1996) Recent apparent changes in relationships between the El Niño-Southern Oscillation and Australian rainfall and temperature. Geophys Res Lett 23:3357–3360. https://doi.org/10.1029/96GL03166

Nogués-Paegle J, Mo KC (1997) Alternating wet and dry conditions over south america during summer. Mon Weather Rev 125:279–291. https://doi.org/10.1175/1520-0493

Penalba OC, Bettolli ML, Krieger PA (2013) Surface circulation types and daily maximum and minimum temperatures in Southern la plata basin. J Appl Meteorol Climatol 52:2450–2459. https://doi.org/10.1175/JAMC-D-13-039.1

Pena-Ortiz C, Gallego D, Ribera P et al (2013) Observed trends in the global jet stream characteristics during the second half of the 20th century. J Geophys Res Atmos 118:2702–2713. https://doi.org/10.1002/jgrd.50305

Pezzi LP, Quadro MFL, Souza EB et al (2023) Oceanic SACZ produces an abnormally wet 2021/2022 rainy season in South America. Sci Rep 13:1455. https://doi.org/10.1038/s41598-023-28803-w

Polvani LM, Previdi M, Deser C (2011) Large cancellation, due to ozone recovery, of future Southern Hemisphere atmospheric circulation trends. Geophys Res Lett. https://doi.org/10.1029/2011GL046712

Reboita MS, Ambrizzi T, Crespo NM et al (2021) Impacts of teleconnection patterns on South America climate. Ann N Y Acad Sci 1504:116–153. https://doi.org/10.1111/nyas.14592

Risbey JS, Pook MJ, McIntosh PC et al (2009) On the remote drivers of rainfall variability in Australia. Mon Weather Rev 137:3233–3253. https://doi.org/10.1175/2009MWR2861.1

Rodrigues RR, Woollings T (2017) Impact of atmospheric blocking on South America in Austral Summer. J Clim 30:1821–1837. https://doi.org/10.1175/JCLI-D-16-0493.1

Rusticucci M, Barrucand M, Collazo S (2017) Temperature extremes in the Argentina central region and their monthly relationship with the mean circulation and ENSO phases. Int J Climatol 37:3003–3017. https://doi.org/10.1002/joc.4895

Santer BD (2003) Behavior of tropopause height and atmospheric temperature in models, reanalyses, and observations: Decadal changes. J Geophys Res 108:4002. https://doi.org/10.1029/2002JD002258

Sarachik ES, Cane MA (2010) The El Niño-Southern Oscillation Phenomenon. Cambridge University Press, Cambridge

Seidel DJ, Randel WJ (2007) Recent widening of the tropical belt: evidence from tropopause observations. J Geophys Res 112:D20113. https://doi.org/10.1029/2007JD008861

Sen PK (1968) Estimates of the regression coefficient based on Kendall's Tau. J Am Stat Assoc 63:1379. https://doi.org/10.2307/2285891

Silva VBS, Berbery EH (2006) Intense Rainfall Events Affecting the La Plata Basin. J Hydrometeorol 7:769–787. https://doi.org/10.1175/JHM520.1

Simmons AJ (2022) Trends in the tropospheric general circulation from 1979 to 2022. Weather Climate Dynamics 3:777–809. https://doi.org/10.5194/wcd-3-777-2022

Smirnov N (1948) Table for estimating the goodness of fit of empirical distributions. Ann Math Stat 19:279–281

Son S-W, Gerber EP, Perlwitz J et al (2010) Impact of stratospheric ozone on Southern Hemisphere circulation change: a multimodel assessment. J Geophys Res 115:D00M07. https://doi.org/10.1029/2010JD014271

Spearman C (1904) The proof and measurement of association between two things. Am J Psychol 15:72. https://doi.org/10.2307/1412159

Thompson DWJ, Solomon S, Kushner PJ et al (2011) Signatures of the Antarctic ozone hole in Southern Hemisphere surface climate change. Nat Geosci 4:741–749. https://doi.org/10.1038/ngeo1296

Trenberth KE, Branstator GW, Karoly D et al (1998) Progress during TOGA in understanding and modeling global teleconnections associated with tropical sea surface temperatures. J Geophys Res Oceans 103:14291–14324. https://doi.org/10.1029/97JC01444

Vasconcellos FC, Deng Y, Zhang H, Martins G (2020) Austral summer precipitation biases over tropical South America in five CMIP5 earth system models. Int J Climatol 40:6506–6525. https://doi.org/10.1002/joc.6595

Vasconcelos Junior F, das C, Jones C, Gandu AW (2018) Interannual and Intraseasonal Variations of the Onset and Demise of the Pre-Wet Season and the Wet Season in the Northern Northeast Brazil. Revista Brasileira de Meteorologia 33:472–484. https://doi.org/10.1590/0102-7786333007

Vera C, Higgins W, Amador J et al (2006) Toward a unified view of the American monsoon systems. J Clim 19:4977–5000. https://doi.org/10.1175/JCLI3896.1

Verdon DC, Franks SW (2006) Long-term behaviour of ENSO: Interactions with the PDO over the past 400 years inferred from paleoclimate records. Geophys Res Lett 33:L06712. https://doi.org/10.1029/2005GL025052

Waugh DW, Banerjee A, Fyfe JC, Polvani LM (2020) Contrasting recent trends in Southern Hemisphere Westerlies across different ocean basins. Geophys Res Lett. https://doi.org/10.1029/2020GL088890

WMO (2018) Scientific assessment of ozone depletion: 2018. Global Ozone Research and Monitoring Project – Report No. 58. Geneva, Switzerland, 588 pp. ISBN: 9781732931718

Woollings T, Blackburn M (2012) The North Atlantic jet stream under climate change and its relation to the NAO and EA Patterns. J Clim 25:886–902. https://doi.org/10.1175/JCLI-D-11-00087.1

Woollings T, Drouard M, O'Reilly CH et al (2023) Trends in the atmospheric jet streams are emerging in observations and could be linked to tropical warming. Commun Earth Environ 4:125. https://doi.org/10.1038/s43247-023-00792-8

Xian T, Homeyer CR (2019) Global tropopause altitudes in radiosondes and reanalyses. Atmos Chem Phys 19:5661–5678. https://doi.org/10.5194/acp-19-5661-2019

Xie P, Chen M, Yang S et al (2007) A gauge-based analysis of daily precipitation over East Asia. J Hydrometeorol 8:607–626. https://doi.org/10.1175/JHM583.1

Yang S, Webster PJ (1990) The Effect of summer tropical heating on the location and intensity of the extratropical westerly jet streams. J Geophys Res 95:18705. https://doi.org/10.1029/JD095iD11p18705

Young PJ, Davis SM, Hassler B et al (2014) Modeling the climate impact of Southern Hemisphere ozone depletion: The importance of the ozone data set. Geophys Res Lett 41:9033–9039. https://doi.org/10.1002/2014GL061738

Zamboni L, Mechoso CR, Kucharski F (2010) Relationships between Upper-Level Circulation over South America and Rainfall over Southeastern South America: a physical base for seasonal predictions. J Clim 23:3300–3315. https://doi.org/10.1175/2009JCLI3129.1

Zolotov SYu, Ippolitov II, Loginov SV, Kharyutkina EV (2018) Variability of the Southern Hemisphere subtropical jet stream in the second half of the 20th century and early 21st century. Izv Atmos Ocean Phys 54:430–438. https://doi.org/10.1134/S0001433818050146